Aerosol absorption by in-situ filter-based photometer and ground-based sun-photometer in a Po valley urban atmosphere

Alessandro Bigi[1], Giorgio Veratti[1,2], Elisabeth Andrews[3,4], Martine Collaud Coen[5], Lorenzo Guerrieri[6], Vera Bernardoni[7], Dario Massabò[8], Luca Ferrero[9], Sergio Teggi[1], and Grazia Ghermandi[1]

[1]Department of Engineering ‘Enzo Ferrari’. University of Modena and Reggio Emilia, 41125 Modena, Italy
[2]ARPAE, Regional Environmental Agency of Emilia-Romagna, 40122 Bologna, Italy
[3]Cooperative Institute for Research in Environmental Sciences, University of Colorado, Boulder (CO), 80309, USA
[4]NOAA Global Monitoring Laboratory, Boulder (CO), 80305, USA
[5]Federal Office of Meteorology and Climatology, MeteoSwiss, 1530 Payerne, Switzerland
[6]National Institute of Geophysics and Volcanology, ONT, 00143 Rome, Italy
[7]Department of Physics, Università degli Studi di Milano and National Institute of Nuclear Physics INFN-Milan, 20133 Milan, Italy
[8]Department of Physics, Università degli Studi di Genova and National Institute of Nuclear Physics INFN-Genoa, 16146 Genoa, Italy
[9]GEMMA and POLARIS Centre, Department of Earth and Environmental Sciences, University of Milano-Bicocca, 20126 Milan, Italy

Correspondence: Alessandro Bigi (alessandro.bigi@unimore.it)

Abstract. Light Absorbing Aerosols (LAA) are short-lived climate forcers with a significant impact on Earth~~radiative balance and~~ 's radiative balance. LAA include dust aerosols, Black Carbon (BC) and organic light-absorbing carbonaceous aerosol (collectively termed as Brown Carbon, BrC), which have been also proven to be highly toxic. ~~Aerosol~~ In this study aerosol absorption at 5 wavelengths (~~UV, B, G, R, IR) by filter photometer~~ ranging from ultraviolet to infrared) was monitored continuously by filter photometer during two winter seasons in 2020 and 2021 in the city of Modena (~~South-central~~ south-central Po valley, ~~Northern~~ northern Italy) at ~~the~~ two regulatory air quality monitoring sites, along with other pollutants (PM_{10}, $PM_{2.5}$, O_3, NO, NO_2, C_6H_6) and vehicular traffic rate. ~~Columnar levels of AODand of other~~ Aerosol Optical Depth (AOD) and other column aerosol optical properties were concurrently monitored at ~~multiple wavelengths by a local~~ four wavelengths by an AERONET sun-photometer at urban background conditions ~~and within the AERONET network~~within Modena. In-situ absorption levels were apportioned both to sources (fossil fuel, biomass burning) and to species (BC, BrC), while columnar absorption was apportioned to BC, BrC and mineral dust. The combined analysis of the atmospheric aerosol and gas ~~levels~~ measurements and of the meteorological conditions (in-situ and by ERA5 reanalysis) identified the location of potential urban sources for BC and BrC, most likely related to traffic and biomass burning. In-situ data ~~shown~~ show different diurnal/weekly patterns for BrC by biomass burning and BC by traffic, with minor differences ~~among~~ between the background and the traffic urban conditions. AERONET version 3 Absorption Aerosol Optical Depth (AAOD) retrievals at 4 wavelengths allowed the estimate of the ~~Absorptive Direct Radiative Effect~~ absorptive direct radiative effect by LAA over the same period under the reasonable assumption that the AOD signal is ~~built up~~ concentrated within the mixing layer. AERONET retrievals showed a modest correlation of columnar absorption with PBL-scaled in-situ observations, although the correlation improves signifi-

cantly during a desert dust transport event ~~, affecting~~ that affected both in-situ aerosol and columnar absorption, particularly in the ~~Blue~~ blue spectrum range. Low correlation occurred between the contribution of BrC to aerosol absorption for the in-situ and the columnar observations, with ~~this~~ the BrC contribution being generally larger ~~at the former~~for in-situ observations. Finally, ~~evidences of a strongly~~ evidence of a highly layered atmosphere during the study period, ~~featured by large~~ featuring significant spatial mixing and modest vertical mixing, were shown by ERA5-based atmospheric temperature profiles and by the large correlation of concurrent AERONET AOD retrievals in Modena and in Ispra (on the NW side of the Po valley, ca. 225 km distant from Modena).

1 Introduction

Light Absorbing Aerosols (LAA) include: dust aerosols; soot-like, graphitic, elemental carbonaceous ~~particles~~ light-absorbing particles qualitatively named Black Carbon (BC)~~, often experimentally reported as equivalent Black Carbon (eBC, Petzold et al., 2013) which~~ . A wide range of experimental techniques are available for the experimental measurement of BC, relying on different properties of LAA. In order to harmonize the terminology used reporting the concentration of this species, the scientific community recommends to report BC observations based on light absorption as equivalent BC (eBC, Petzold et al., 2013). eBC aerosol particles have fairly constant ~~absorption across the~~ refractive index across the ultraviolet – infraredUV – IR~~range (Moosmüller et al., 2009); and the radiation absorbing fraction of organic aerosol named Brown Carbon (BrC, Andreae and Gelencsér, 2006; Laskin et al., 2015),~~ range (Moosmüller et al., 2009). The eBC concentrations are converted into light-absorbing carbon mass concentration using the mass-specific absorption cross section (MAC). Another type of LAA is Brown Carbon (BrC, Andreae and Gelencsér, 2006; Laskin et al., 2015) which is the fraction of light-absorbing organic aerosol whose optical properties differ from those of BC, because of their enhancement in absorption towards UV wavelengths.

LAA are short-lived climate forcers ($\sim$ 1 week atmospheric residence time (Forster et al., 2021)) and significantly affect the Earth radiative balance (Bond et al., 2013; Wang et al., 2016a). In terms of global impact, BC was shown to have a positive ~~Direct Radiative Effect~~ direct radiative effect at the Top-Of-Atmosphere (TOA) ~~ranging between~~ in the range of 0.71 – 0.82 $\mathrm{W m^{-2}}$ (Chung et al., 2012; Bond et al., 2013; Lin et al., 2014)~~, while the BrC~~ . Estimates of global direct effect ~~resulted is lower , with larger spatial variability over the Earth and~~ were lower for BrC than for BC, in the range of 0.04 – 0.57 $\mathrm{W m^{-2}}$ (Feng et al., 2013; Lin et al., 2014; Saleh et al., 2014; Jo et al., 2016; Brown et al., 2018; Zhang et al., 2020)~~,~~ ~~depending~~ . BrC concentrations are very spatially variable and concentrations depend on the study specifics. Due to ~~the large~~ aerosol-cloud interactions, the overall ~~Effective Radiative Forcing~~ effective radiative forcing of LAA (i.e. the difference in their radiative effect between the present day and pre-industrial times (Heald et al., 2014)) ranges between 0.15 ± 0.17 $\mathrm{W m^{-2}}$ for BC (Thornhill et al., 2021; Forster et al., 2021), with the largest part of this uncertainty arising mainly from the indirect and semi-direct effect exerted by aerosol on cloud condensation nuclei, ice nuclei and on the atmospheric lapse rate, along with the aerosol mixing state (Twomey, 1974; Charlson et al., 1992; Bond et al., 2013; Rosenfeld et al., 2014; Takemura and Suzuki, 2019).

In addition to the effects on climate, the scientific literature has documented the adverse effects on human health of aerosol, which significantly affects life expectancy ~~(Cohen et al., 2017; Loomis et al., 2013; West et al., 2016)~~ (Loomis et al., 2013; Cohen et al., 2017; West et al., 2016). The toxicological effect of particulate matter (PM) is known to depend on the aerosol size distribution and chemical composition (Pöschl, 2005). BC is one of the components with a ~~proved~~ proven harmful effect on human health (Janssen et al., 2012), and both long-term and acute exposure to increased eBC concentrations have been shown to increase the mortality risk (Ostro et al., 2015; Yang et al., 2021). Recent studies have also ~~proven~~ shown that the exposure to increased eBC concentrations were positively associated with various health issues such as ischemic heart disease and myocardial infarction ~~(Kirrane et al., 2019; Luben et al., 2017; Magalhaes et al., 2018)~~ (Luben et al., 2017; Magalhaes et al., 2018; Kirrane et al., 2019). In addition, Regencia et al. (2021) observed that short-term cumulative exposure to traffic-related eBC concentrations could adversely affect blood pressure, resulting in cardiovascular diseases. BrC has also been shown to have detrimental health effects, enhanced because of its enrichment in organic compounds (Chowdhury et al., 2019; Offer et al., 2022), possibly related to aerosol aging (Li et al., 2022; Tuet et al., 2017; Weitekamp et al., 2020).

The compilation of reliable and accurate emission inventories for eBC is critical for the development of robust air quality control strategies and the mitigation of global warming. However, the large uncertainty associated with source emission factors~~and PM speciation makes it difficult to implement~~ , PM speciation and eBC definition makes the implementation of systematic and harmonized emission estimates ~~at national and regional levels~~a challenging task. Despite these limitations, most studies identify road transport as the largest eBC emission source in Europe (Wang, 2015), followed by biomass burning and industry (European Environment Agency, 2013), as more recently confirmed by the analysis of the eBC emission change in Europe due to COVID-19 lockdowns (Evangeliou et al., 2021). Similar to BC, BrC can be directly emitted into the atmosphere during the combustion of fossil fuels, although its major source is biomass burning. BrC can also originate from secondary reactions, e.g. through ~~ageing~~ aging processes or by photo-oxidation of biogenic or anthropogenic volatile organic compounds (Laskin et al., 2015).

Several approaches have been proposed in the literature to measure LAA, including photothermal interferometry, photoacoustic spectroscopy, and on-line or off-line filter-based light attenuation methods (Lack et al., 2014). The difference in the BC reported by these techniques increases when significant amounts of secondary organic are present (Kalbermatter et al., 2022). Both the interferometric and the acoustic approaches can be considered thermal based measurements, since they quantify the fraction of absorbed optical energy that is rapidly transferred into the surroundings under a controlled light source emission. The main advantage of these techniques is their direct measurement of the absorption of particles while suspended in air, however they both suffer from technical and operational limitations. For example, the photo-acoustic technique is very sensitive to atmospheric conditions such as relative humidity, temperature and pressure (Langridge et al., 2013), while photothermal interferometry is sensitive to mechanical vibration, although it has recently gained new attention ~~(e.g. Drinovec et al., 2022; Visser et al., 2020)~~(e.g. Visser et al., 2020; Drinovec et al., 2022). Filter-based measurements are very simple to operate, but have the main disadvantages of filter-related artifacts, such as the filter loading and the multiple scattering effects within filter fibres and between the collected particles and the filter fibres, possibly leading to systematic errors in the measurements. With the aim to overcome these limits, different technical and analytical corrections have been developed to correct for ~~these~~ the non-idealities of filter-based measurements (e.g. Weingartner et al., 2003; Petzold et al., 2005; Virkkula et al., 2007; Collaud Coen et al., 2010; Hyvärinen et al., 2013; Drinovec et al., 2015; Li et al., 2020), ~~making the use of~~ for filter absorption photometers common in field experiments and in air quality monitoring networks. The aethalometer (Magee Scientific Co., Berkeley, USA), is a commonly used filter-based photometer designed to measure LAA at multiple wavelengths and at high temporal resolution, generally at fixed monitoring sites. Lightweight portable micro-aethalometers, such as the AE51 or the MA200 series (Aethlabs, San Francisco, USA), were recently developed and successfully used in complex urban environments for pedestrian exposure assessments ~~(Boniardi et al., 2021; Good et al., 2017; Viana et al., 2015)~~ (Viana et al., 2015; Good et al., 2017; Boniardi et al., 2021), mobile observations ~~(Grivas et al., 2019; Liu et al., 2021, 2019)~~ (Grivas et al., 2019; Liu et al., 2019, 2021) and vertical profile investigations through unmanned aerial vehicles (UAVs) ~~or balloons (Kezoudi et al., 2021; Pikridas et al., 2019; Ferrero et al., 2011, 2014)~~ and balloons (Ferrero et al., 2011, 2014; Pikridas et al., 2019; Kezoudi et al., 2021). Despite their limitations, multi-wavelength aerosol absorption observations by filter photometers have proven suitable for the application of source and component apportionment models, such as the 'Aethalometer model' (Sandradewi et al., 2008) to apportion BC between wood burning and fossil fuel combustion emissions or the Multi-Wavelength Absorption Analyzer (MWAA, Massabò et al., 2015; Bernardoni et al., 2017) algorithm, which ~~extends the capabilities of the Aethalometer for disentangling the~~ enables disentanglement of the BC and BrC components ~~, and consistently determining~~ of LAA, and a determination of their radiative forcing (Ferrero et al., 2021a).

Surface in-situ aerosol measurements can provide important information about aerosol characterization and concentration for the lowest tropospheric layer~~, however,~~. However, estimating the vertical distribution of aerosol particles or their columnar load remains crucial to completely ~~understand~~ understanding their impact on the climate system. In order to meet this need, the worldwide network of calibrated sun/sky photometers AErosol RObotic NETwork (AERONET, Holben et al., 1998) was developed, with the goal of measuring aerosol optical columnar properties, e.g. aerosol optical depth (AOD) and column single-scattering albedo (SSA). Numerous studies have attempted to compare in-situ observations with ground-based columnar aerosol optical properties providing different results depending on the atmospheric mixing state, the aerosol vertical profile and the local/regional pollution conditions. Several authors ~~found the boundary-layer-scaled~~ used the ratio between the surface in-situ ~~atmospheric extinction underestimated sun photometry observations of both AOD and~~ aerosol mass concentration or aerosol absorption and the boundary-layer-height (i.e. they rescaled surface data over this atmospheric layer), and showed how this ratio underestimated sun-photometry observations of AOD or absorption AOD (AAOD) ~~(e.g. Bergin et al., 2000; Aryal et al., 2014; Chauvigné et al., 2016; Slater and Dibb, 2004; Chen et al., 2019), in~~ respectively (e.g. Bergin et al., 2000; Slater and Dibb, 2004; Aryal et al., 2014; Chauvigné et al., 2016; Chen et al., 2019). These findings were consistent across various types of locations (e.g. rural background, moderately polluted or marine) ~~. These previous studies~~ and highlighted that, in those settings, generally the main factors limiting the representativity ~~by~~ of surface in-situ measurements of the atmospheric column are the aerosol mixing within the boundary layer (BL) and the presence of aerosol above the BL, which can ~~significantly contribute~~ contribute significantly to the extinction and absorption in the column.

Datasets allowing a worldwide trend analysis in LAA levels remain limited (Laj et al., 2020), however according to both in-situ (Collaud Coen et al., 2020) and ground-based columnar (Li et al., 2014) observations, in the ~~Northern~~ northern hemisphere, particularly in the US and Europe, the aerosol absorption coefficient (σ_{ap}) decreased over the last decade(s). More specific to the ~~study area reported here, a decrease in Ispra (Italy), on the NW side of the Po valley, was observed~~ region of interest for our study, the Po valley is a European hot-spot for atmospheric pollution situated in northern Italy. A previous work on the Po basin observed a decrease for both columnar AOD and in-situ aerosol scattering and absorption ~~(Putaud et al., 2014) in the~~ in Ispra, on the NW side of the Po valley, in the early 2000s (Putaud et al., 2014). This drop was consistent with a significant valley-wide decrease in PM_{10} and $\mathrm{PM}_{2.5}$ in-situ ground levels (Bigi and Ghermandi, 2014, 2016), thanks also to a drop in primary PM emissions by vehicular transport. ~~Significant~~ Similarly, a drop of ~4% per year over the period 1997 – 2016 was recorded for the elemental carbon content in fog samples at the rural background site of San Pietro Capofiume (Gilardoni et al., 2020b).

Significant aerosol sources other than traffic remain present in the valley, ~~as shown by~~ e.g. biomass burning by domestic heating for several compounds including organic aerosols and BC, and farming for NH_3, a major PM precursor. Their role in PM levels was highlighted by the small decrease in PM across the basin (Ciarelli et al., 2021; Putaud et al., 2021) and in particle count in Modena (Shen et al., 2021) during the 2020 lockdown due to the SARS-CoV-2 pandemics. ~~Previous~~ Some studies in the Po valley addressed temporal and vertical variability of σ_{ap} in Milan, the largest city of the basin ~~(Ferrero et al., 2014, 2011; Vecchi et al., 2018)~~(Ferrero et al., 2011, 2014; Vecchi et al., 2018). These authors found a decline in BC levels within the mixing layer, with higher BC levels observed at the ground (i.e. 50 – 100 m) and a marked drop (more than 50%) above the mixing height, with BC contributing to ∼10% (∼8%) of the overall PM_1 extinction (mass) at a surface Milan urban background site in winter. Other studies in the Po valley focused on the effect of the reduction in $\mathrm{NO_x}$ and NH_3 on $\mathrm{PM}_{2.5}$ levels (Veratti et al., 2023), as well as on the impact of biomass burning on surface aerosols, particularly at the rural background site of San Pietro Capofiume and the urban site of Bologna (Gilardoni et al., 2016; Costabile et al., 2017; Paglione et al., 2020)~~, highlighting~~. These latter studies highlighted the large Absorption Ångström Exponents (AAE, Moosmüller et al., 2009) for biomass burning organic aerosol, ranging from ∼3 – ~~5. They found larger AAE~~5, mainly due to aged aerosols in the aqueous phase and related to an increase in the organic aerosol/BC mass ratio. Previous investigations of the spatial variability of PM surface observations highlighted the impact of large urban areas on aerosol load, particularly for PM_{10}~~(Bigi and Ghermandi, 2014, 2016).~~, using cluster analysis (Bigi and Ghermandi, 2014, 2016). A Europe-wide assessment of urban air quality by Thunis et al. (2017), based on a simplified dispersion model, estimated a 57% contribution by in-city emissions to urban $\mathrm{PM}_{2.5}$ in Milan, making this city the one with the largest self-contribution to local $\mathrm{PM}_{2.5}$ across the European Union. Similarly the spatial variability in columnar aerosol load observed by ground-based remote sensing instruments between Ispra and the Adriatic sea, east of the Po basin, showed larger AOD and lower SSA at the Ispra site (Clerici and Mélin, 2008), confirming the impact of in-valley combustion emissions.

~~The present~~ Relying on these previous findings, the current study provides additional knowledge on LAA ~~behaviour~~ in the Po ~~Valley (an European hot-spot for atmospheric pollution)~~ valley by investigating the temporal, spatial and columnar variability of σ_{ap} ~~during winter 2020 – 2021 using in-situ and ground-based columnar observations~~ in Modena, ~~a mid-size urban area in the~~ an urban area representative of several cities in the basin. The city of Modena is located in the central-south part of the

Po ~~valley and representative of several cities in the basin~~Valley. The study period is winter 2020 – 2021 and the experimental dataset includes both in-situ and ground-based columnar observations. Additionally, source apportionment of σ_{ap} using the in-situ and the ground-based columnar observations in Modena are compared to investigate the impact of low level emissions and long range transport on the aerosol optical properties, together with the first estimation of LAA heating rate (HR) and its diurnal trend in Modena. Finally, more insight into the spatial and temporal variability of the different absorbing components in the Po valley are provided by a comparison between columnar optical properties in Modena and Ispra. Below we first describe the measurements we will use and then address these topics.

2 ~~Materials~~ Measurement site and methods

Modena (44.6° N, 10.9° E, 32 m a.s.l., ~ 180 000 inhabitants) is located on the ~~southeast~~ centre-south side of the Po valley~~in Northern~~, in northern Italy, a basin surrounded by the Alps and the Apennines. The basin area is affected by recurrent atmospheric temperature inversions in winter and low wind conditions, leading to a build-up of atmospheric ~~pollutant concentration~~pollutants. The result is that the Po valley is one of the largest European regions exceeding the daily PM_{10} limits set by the European regulation (EC 50/2008) and by the ~~WHO guidelines (2021)~~ World Health Organisation (WHO) guidelines (WHO, 2021). The city is situated in flat topography, 13 km north of the foot of the closest Apennine hills and 96 km south of the foot of the Alps, i.e. it is on the Southern side of a wide (~ 110 km) valley.

The latest bottom-up regional emission inventory for the area of the municipality of Modena (ARPAE, 2020), reference year 2017, identifies traffic and domestic heating as the main PM_{10} sources, contributing 38% and 58% of total emissions respectively, although Modena also hosts a few districts for light manufacturing (Selected Nomenclature for sources of Air Pollution, SNAP 3 and 4), contributing 3% of total PM_{10} emissions (Figure 1). More specific to non-industrial combustion (SNAP 2), most of buildings use compressed natural gas for both heating and cooking; consistently 99.4% of PM_{10} emissions by SNAP 2 are estimated to be produced by biomass combustion for domestic heating (ARPAE, 2020).

As is common to most urban areas in the basin, vehicular traffic is the main source of NO_x emissions (78% of total NO_x emissions, ARPAE, 2020), with a significant impact on local air quality (Ghermandi et al., 2020; Veratti et al., 2020) and on population exposure (Veratti et al., 2021). Modena's setting is ~~representative of~~ quite representative of several mid-size urban areas across the Po valley, ~~making Modena a model for mid-size urban areas across the basin which host about one third of the population of the valley~~particularly in terms of traffic and domestic emissions sources and topography.

2.1 In-situ surface measurements

Two MA200 micro-aethalometers were installed in Modena, sampling from the gently heated (~ 30 ±2 °C) glassware manifold inlet lines already in use ~~also~~ for reactive gas monitors at the two regulatory air quality monitoring sites in town: Giardini (EoI code IT0721A, 44.637° N, 10.906° E, 39 m a.s.l.) and Parco Ferrari (EoI code IT1771A, 44.652° N, 10.907° E, 30 m a.s.l). These two sites are representative of urban traffic and urban background conditions, hereafter referred as UT and UB

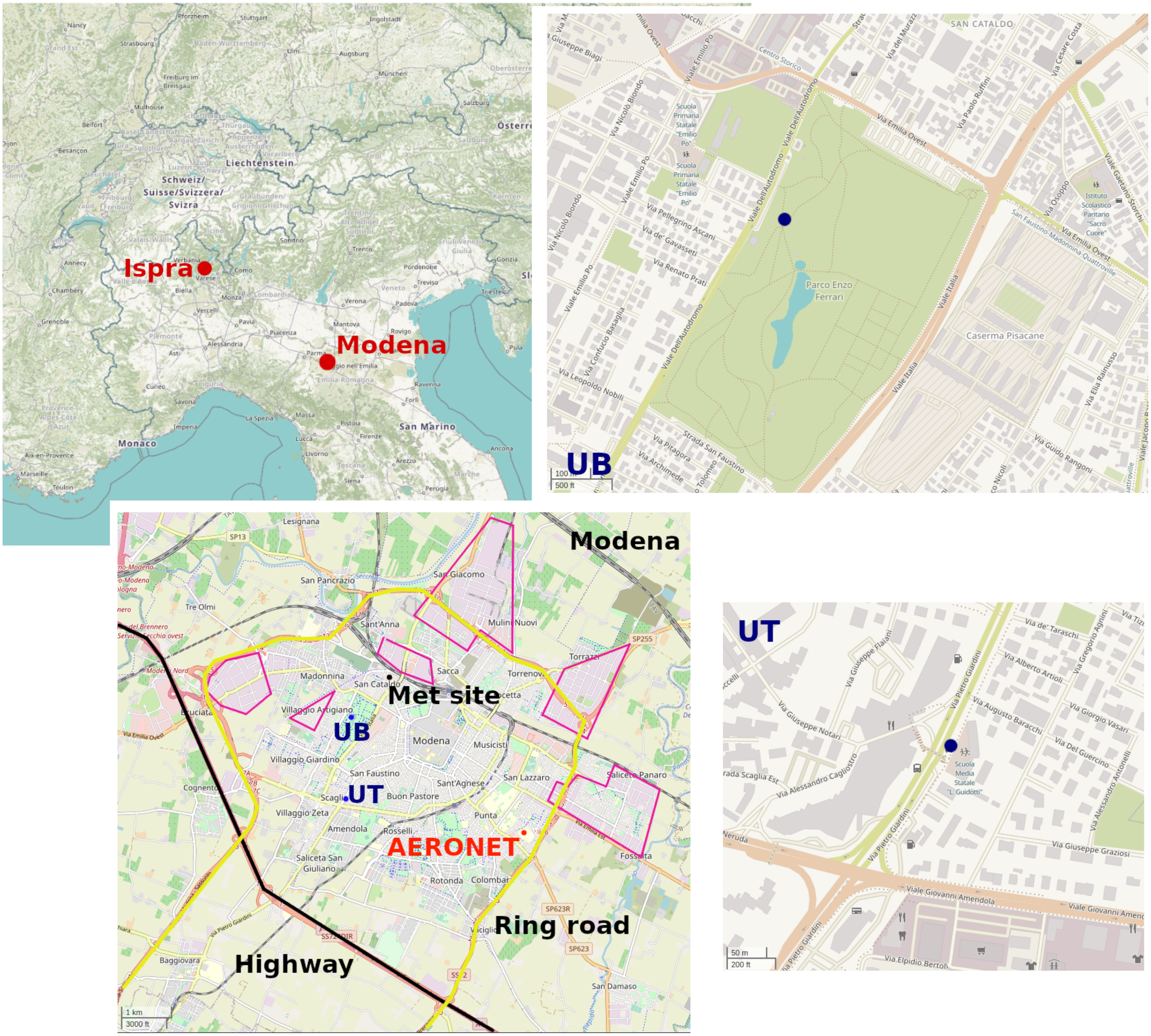

Figure 1. Setting of the measurement site. Areas outlined in purple indicate the manufacturing districts (from © OpenStreetMap contributors 2023. Distributed under the Open Data Commons Open Database License (ODbL) v1.0.).

respectively (see Figure 1 for their location). The ~~inlet height~~ UT site faces a major road with two lanes per direction, with estimated median daily traffic counts of ~20 thousand vehicles, while the UB is within Modena's largest urban park at a distance of ~120 metres from the nearest road. The inlet height at both sites is approximately 4 m above ground. The inlet has no size cut, i.e. the instruments are sampling total suspended particles.

The MA200 are filter absorption photometers measuring at 5 wavelengths (λ = 375 nm, 470 nm, 528 nm, 625 nm, 880 nm) using PTFE filter tapes. AAE for in-situ observations (hereafter AAE^{i}) was computed by a fit to absorption at all 5 wavelengths. The instruments were used in dual-spot sampling mode (firmware 1.09 and 1.10 were installed during the study) and a compensation algorithm similar to the one proposed by Drinovec et al. (2015) is applied by the internal firmware. This firmware uses a multiple scattering correction coefficient C_{ref} = 1.3, which was chosen by the manufacturer in order to mimic the response by the Aethalometer AE33 (Aethlabs, personal communication).

Aerosol absorption monitoring at the UT site was performed between 19 January – 21 April 2020 and 9 November 2020 – 8 March 2021 with a time resolution of 1 minute. At the UB site, aerosol absorption was monitored between 4 February 2020 – 13 October 2020 at 1 minute time resolution and between 13 December 2020 – 20 March 2021 at a 5 minute time resolution. In order to compensate for the occasionally low absorption readings at the latter site, the 1-minute ~~data at UB was~~ raw transmittance counts at UB were firstly aggregated to 5 minutes ~~by a custom application of the AE33~~ and then used to compute the corresponding σ_{ap} by a transcription in R programming language of the dual-spot compensation ~~(Drinovec et al., 2015) on the raw transmittance counts.~~ algorithm as described in Drinovec et al. (2015). The MA200 measurements were screened depending on the status reported by the instrument. Flow calibration was performed before each filter change. Flow was set to $100\ \mathrm{ml\,min^{-1}}$ ~~and~~ in winter and increased to $125\ \mathrm{ml\,min^{-1}}$ in ~~winter and summerrespectively~~summer, because of the lower atmospheric concentrations. In the present study only measurements from winter months were analyzed, i.e. December, January and February. Strict lockdown restrictions in Northern Italy due to the SARS-CoV-2 pandemic lasted from 8 March 2020 until 4 May 2020, therefore the winter data reported here are representative of a business-as-usual scenario, partly spanning across two winter seasons. Absorption data were averaged to 1 hour prior to the analysis, in order to match the time resolution of other analyzed variables.

A comprehensive uncertainty analysis for absorption observations by the MA200 has not yet been fully performed by the scientific community. Li et al. (2021) looked at the multiple scattering uncertainty of its PTFE filter and suggested that multiple scattering artifacts might lead to an overestimation of the absorption by BrC, with the bias dependent on the absorbing strength of the compound, i.e. a behaviour qualitatively similar to that of the AE33 (Yus-Díez et al., 2021). Alas et al. (2020) performed a large intercomparison involving these devices, testing several MA200s (single spot, 10 s and 60 s time resolution) and highlighted a low unit-to-unit variability (ca. 2%) across all wavelengths and good agreement ($R^2 > 0.93$) for loading-corrected eBC when compared to the AE33. In the current study a 8% uncertainty was attributed to MA200 absorption, based on the mean standard error of the slope of the linear regression between the eBC by the MA200 and the AE33 found by Alas et al. (2020).

Regulatory air quality data were also available at the two sites and include NO, NO_2, O_3 (UB site only), and C_6H_6 (UT site only) at hourly time scale~~;~~. PM_{10} and $PM_{2.5}$ (at UB site only) were also available, although on a daily time scale. ~~Additionally, direct~~ The daily PM_{10} median (10th, 90th quantiles) concentration at the UB site over the period 2017 – 2021 was 24 $\mu g\,m^{-3}$ (13 $\mu g\,m^{-3}$, 57 $\mu g\,m^{-3}$), while at the UT site the same statistics for PM_{10} were 27 $\mu g\,m^{-3}$ (14 $\mu g\,m^{-3}$, 63 $\mu g\,m^{-3}$). Consistently, over the same period, hourly NO_2 at the UB showed lower levels than at the UT site, with the two locations having a median (10th, 90th quantiles) of 23 $\mu g\, m^{-3}$ (6 $\mu g\, m^{-3}$, 50 $\mu g\, m^{-3}$) and 35 $\mu g\, m^{-3}$ (14 $\mu g\, m^{-3}$, 66 $\mu g\, m^{-3}$) respectively.

Direct traffic counts were also available for the urban area during the period of investigation. These data were collected by 400 induction loops for traffic light control within the urban and suburban street network. Continuous vehicle counts from the induction loops nearest to the UT and UB sites were aggregated into one hour total traffic data; these hourly aggregates were used primarily to highlight variability in traffic patterns. The uncertainty in the count by these devices is approximately 10% (Bellucci and Cipriani, 2010).

Meteorological variables were provided by the regional weather monitoring network station within the urban area of Modena, and include wind speed and direction (WS, WD), atmospheric temperature (T), relative humidity (RH), downward global radiation (Q) and atmospheric pressure (p). The site is on the roof of the municipality offices at 40 meters above ground and is the highest weather station in the urban area with data available over the study period. These data provide indications of the wind conditions inside the urban canopy, but may differ from wind conditions at the 4 m height of the MA200 measurement.

2.2 Mixing layer height

Hourly estimates for the mixing layer height (MLH) were provided by ERA5 reanalysis ~~(Hersbach et al., 2018).~~(Hersbach et al., 2018). ERA5 reanalysis, provided by the European Centre for Medium-Range Weather Forecasts (ECMWF), proceeds from the data assimilation of global observations into the Integrated Forecast System (IFS), a global numerical weather prediction model, to produce a globally complete and consistent dataset of physical quantities, continuous in time and space. ERA5 provides hourly estimates for several geophysical quantities, including MLH, at a grid resolution 0.25° × 0.25° over the period 1940 - today. For this study we extracted the MLH at the ERA5 grid point with coordinates 11.00° W, 44.75° N. Modena is about 14 km south of this grid point, i.e. it lays between two ERA5 grid points, since in this region the size of the ERA5 cell is ~20 km × ~28 km: MLH was extracted at that grid point since it is representative of a cell over an area with flat topography, i.e. very similar to the area of Modena. MLH estimates by ERA5 are used in the analysis, since no experimental estimates of the planetary boundary layer height were available in town and the closest location with regular atmopsheric sounding (at 12 UTC and 00 UTC) is in San Pietro Capofiume, a rural background site surrounded by a flat topography 53 km east of Modena. The ERA5 estimate of MLH in Europe was assessed to be underestimated on average (median) by ~54 m (~19 m) based on a comparison between ERA5 and daytime radiosoundings by Guo et al. (2021). This underestimate represents a lower end estimate, since generally soundings in Europe are taken around 12 UTC, i.e. when the MLH is quite developed.

It is worth noting that deficiencies have been observed in various planetary boundary layer and surface parameterizations for conventional meteorological models (e.g. IFS, WRF, and COSMO. MO. Martilli et al., 2021; Maroneze et al., 2021; Lapo et al., 2019; Battisti et al., 2017), leading to a challenging characterization of strong thermal inversions (Mahrt, 2014; Acevedo et al., 2019) , like those occurring in the Po valley. All these meteorological models typically rely on a single stability parameter, e.g. the Richardson number or the turbulent kinetic energy, to automatically estimate MLH based on fixed thresholds, regardless of the wide range of possible atmospheric conditions, since these models cannot apply *ad-hoc* methods for each individual situation. More specific to this study, MLH estimates by IFS are based on the bulk Richardson number (Vogelezang and Holtslag, 1996), regardless of the atmospheric stability conditions, and MLH is defined as the lowest level at which the bulk Richardson number reaches the critical value of 0.25 (ECMWF, 2017).

2.3 Ground-based columnar measurements

Column-integrated measurements of optical properties of the Modena urban atmosphere were collected by a multi-channel Cimel CE-318 sun/sky photometer installed on the roof of the Dept. of Engineering 'Enzo Ferrari' at about 20 m above the ground. The instrument is part of NASA's AERONET network (Holben et al., 1998). This site, within the grounds of the University campus and representative of residential background conditions, is on the southeastern edge of the urban settlement, while the UB and UT sites are on the west side of the town at a distance of 4 km and 3.5 km respectively (Figure 1).

In our analysis of the Cimel data, we considered both Level 2.0 and Level 1.5 version 3 almucantar retrievals at 4 wavelengths (λ = 440, 675, 870, and 1020 nm) (Sinyuk et al., 2020). Level 2.0 absorption data are more robust (e.g., Dubovik et al., 2000), but Level 1.5 data provide more matches with surface measurements, as discussed below. The almucantar retrievals provide several columnar properties including Absorption Aerosol Optical Depth (AAOD), SSA, the depolarization ratio and the lidar ratio at the 4 wavelengths, as well as the particle volume size distribution and AOD apportioned to submicron and supermicron aerosols from which fine mode fraction (FMF) is calculated (O'Neill et al., 2003). AERONET retrievals also allowed estimation of the Scattering AOD (SAOD(λ_j) = Total AOD(λ_j) - AAOD(λ_j)) for each of the 4 wavelengths, and the wavelength dependence of SAOD, i.e., the column Scattering Ångström Exponent (hereafter SAE^c), as well as the column Absorption Ångström Exponent (AAE^c).

There is much information in the literature about the uncertainty in AERONET products (e.g. Eck et al., 1999; Andrews et al., 2017; Sinyuk et al., 2020; Kayetha et al., 2022). A fixed AOD uncertainty set to 0.01 was used, following Eck et al. (1999) . For the current study, AOD-dependent uncertainty in SSA at 440, 675 and 875 nm by AERONET v3 retrievals was estimated based on the data from a urban site in Sinyuk et al. (2020), ranging from 0.017 at 440 nm when AOD_{440} is 0.7 to 0.103 at 870 nm when AOD_{440} is 0.03. The overall uncertainty for the analysed aerosol parameter, e.g. AAOD, was estimated as a propagation of the uncertainties of AOD and SSA and ranged between 0.011 and 0.033.

In addition, the ~~Direct Radiative Effect~~ direct radiative effect (DRE) at the top of the atmosphere (TOA) and bottom (BOA), retrieved by AERONET in clear sky conditions in winter, were considered. Since the atmospheric aerosol is characterized by a significant absorptive capacity the difference between the DRE at TOA and BOA (hereafter Δ DRE_{atm}) represents the instantaneous radiative power density absorbed along the atmospheric column by the aerosol within that atmospheric layer (Chakrabarty et al., 2012; Kedia et al., 2010). Δ DRE_{atm} is expressed in $\mathrm{W\,m^{-2}}$, which is the common metric used in the literature to quantify the integrated radiative power density absorbed by the aerosol in the atmosphere (Kedia et al., 2010; Das and Jayaraman, 2011; Bond et al., 2013; Heald et al., 2014). However, as demonstrated in Ferrero et al. (2014), a more useful parameter is the Absorptive DRE (ADRE) of atmospheric aerosol, which can be computed simply by normalizing Δ DRE_{atm} by the atmospheric thickness Δz hosting most of the LAA, and this thickness in the Po valley can be generally assumed to correspond to the MLH. The ADRE represents the radiative power absorbed by the aerosol for unit volume of the atmosphere ($\mathrm{W\,m^{-3}}$). The advantage of using ADRE in the Po Valley environment in wintertime is that, in this case, most of the AOD signal is built up within the mixing layer, as shown by both Ferrero et al. (2019), who found that in Milan up to 87% of AOD signal was generated within mixing layer~~and~~ , 8% in the residual layer and 5% in the free troposphere, and by Barnaba et al. (2010), who found ~~consistent~~ similar figures at the Ispra background site. This means that if the thickness Δ z is the MLH, the ADRE will refer to that layer with an expected maximum overestimation of approximately ~~15% .~~ 13% (i.e. roughly the amount of aerosol optical depth above the MLH). From the ADRE the instantaneous ~~Heating Rate~~ heating rate (HR, $\mathrm{K\,day^{-1}}$) can be computed as (Ferrero et al., 2014):

$$HR = \frac{\mathrm{ADRE}}{\rho\,\mathrm{C_p}} \tag{1}$$

where ρ is the air density and $\mathrm{C_p}$ (1005 $\mathrm{J\,kg^{-1}\,K^{-1}}$) is the isobaric specific heat of dry air. The most important advantages of this AERONET-based approach to derive the LAA HR are: (a) the possibility of obtaining a rapid HR estimation to investigate the HR temporal evolution ~~on a selected~~ during a selected time period and (b) the possibility of deriving the HR using a well-established network (AERONET) allowing a global comparison of the output. This approach is limited ~~both because the HR is independent of the thickness of the investigated atmospheric layer and because HR~~ because HR can be obtained directly by the AERONET retrievals only if most of the AOD signal is built up within the mixing layer (thus with an expected overestimation of ~~~15~~13%). Due to these limitations, ~~in the present study, retrievals during events of high altitude dust transport were discarded from~~ the analysis of the HR is limited to retrievals collected during days without significant dust content. This screening process followed the same process used for in-situ data described in section 2.4.1, since the apportionment of in-situ data suffered from a similar limitation as that of the HR analysis.

Furthermore, in some of the analysis described below, the in-situ and columnar data were compared, requiring temporal matching of the two data sets. An in-situ/columnar observation match is considered successful when the AERONET retrieval occurred during the hourly averaged in-situ measurement. Level 1.5 version 2 AERONET data are known to have large uncertainty when AOD at 440 nm ($\mathrm{AOD_{440}}$) is less than 0.4 (Dubovik et al., 2000). In order to maximize the availability of columnar measurements for the analysis, Level 1.5 data were used. Level 1.5 data points with $\mathrm{AOD_{440}} \leq 0.2$, were discarded from the analysis and the data remaining after the AOD screening are referred to as L1.5* in what follows.

2.4 ~~Measurement uncertainty~~

~~A comprehensive uncertainty analysis for absorption observations by the MA200 has not yet been fully performed by the scientific community. Li et al. (2021) looked at the multiple scattering uncertainty of its PTFE filter and suggested that multiple scattering artifacts might lead to an overestimation of the absorption by BrC, with the bias dependent on the absorbing strength of the compound, i.e. a behaviour qualitatively similar to that of the AE33 (Yus-Díez et al., 2021). Alas et al. (2020) performed a large intercomparison involving these devices, testing several MA200s (single spot, 10 and 60 time resolution) and highlighted a low unit-to-unit variability (ca. 2%) across all wavelengths and good agreement ($R^2 > 0.93$) for loading-corrected eBC when compared to the AE33. In the current study a 8% uncertainty was attributed to MA200 absorption, based on the mean standard error of the slope of the linear regression between the eBC by the MA200 and the AE33 found by Alas et al. (2020).~~

~~There is much information in the literature about the uncertainty in AERONET products (e.g. Eck et al., 1999; Andrews et al., 2017; Sinyuk et al., 2020; Kayetha et al., 2022). A fixed AOD uncertainty set to 0.01 was used, following Eck et al. (1999). For the current study, AOD-dependent uncertainty in SSA at 440, 675 and 875 nm by AERONET v3 retrievals was estimated based on the data from a urban site in Sinyuk et al. (2020), ranging from 0.017 at 440 nm when AOD~~ ~~$_{440}$~~ ~~is 0.7 to 0.103 at 870 nm when AOD~~ ~~$_{440}$~~ ~~is 0.03. The overall uncertainty for the analysed aerosol parameters, e.g. AAOD, was estimated as a propagation of the uncertainties of AOD and SSA and ranged between 0.011 and 0.033. Finally, uncertainty in MLH was assessed to be ∼ 50 based on a comparison between ERA5 and daytime radiosoundings by Guo et al. (2021), representing a lower end estimate since most of soundings are taken at 12 UTC, i.e. when the MLH is quite developed.~~

2.4 Source apportionment of in-situ columnar data

Both in-situ and columnar data were apportioned according to the aerosol spectral properties, i.e solving the balance of the aerosol absorption based on its dependence on the AAE, on the absorbing species and on the wavelengths. Two different apportionment approaches were used for the in-situ and the columnar observations, although based on the same foundation. The approach applied to the in-situ data requires at least five wavelengths to ensure stability (Bernardoni et al., 2017).

2.4.1 In-situ apportionment

In-situ aerosol absorption σ_{ap} was apportioned to species (Black Carbon, Brown Carbon, referred to as $\sigma_{\mathrm{ap}}^{\mathrm{BC}}(\lambda)$ and $\sigma_{\mathrm{ap}}^{\mathrm{BrC}}(\lambda)$ respectively) and sources (fossil fuel and biomass burning combustion, referred to $\sigma_{\mathrm{ap}}^{\mathrm{ff}}(\lambda)$ and $\sigma_{\mathrm{ap}}^{\mathrm{BB}}(\lambda)$) using the Multi-Wavelength Absorption Analyzer model (MWAA, Massabò et al., 2015; Bernardoni et al., 2017). This model assumes an equivalence between the Absorption Ångström Exponent (AAE, Moosmüller et al., 2009) of BC and that of fossil fuel ($\mathrm{AAE^i}_{\mathrm{BC}} = \mathrm{AAE^i}_{\mathrm{ff}}$), and it assumes biomass burning to be the only source of BrC. ~~To solve the set of equations within the MWAA~~ Under these hypotheses, the MWAA model assumes that both the following equations hold for the total $\sigma_{\mathrm{ap}}(\lambda)$ at each wavelength:

$$\sigma_{\mathrm{ap}} = \sigma_{\mathrm{ap}}^{\mathrm{BC}}(\lambda) + \sigma_{\mathrm{ap}}^{\mathrm{BrC}}(\lambda) = \mathrm{A}\cdot\lambda^{-\mathrm{AAE}^{\mathrm{i}}_{\mathrm{BC}}} + \mathrm{B}\cdot\lambda^{-\mathrm{AAE}^{\mathrm{i}}_{\mathrm{BrC}}} \quad (2)$$

$$\sigma_{\mathrm{ap}} = \sigma_{\mathrm{ap}}^{\mathrm{ff}}(\lambda) + \sigma_{\mathrm{ap}}^{\mathrm{bb}}(\lambda) = \mathrm{A}'\cdot\lambda^{-\mathrm{AAE}^{\mathrm{i}}_{\mathrm{ff}}} + \mathrm{B}'\cdot\lambda^{-\mathrm{AAE}^{\mathrm{i}}_{\mathrm{bb}}} \quad (3)$$

In Equations 2 and 3 $\mathrm{AAE}^{\mathrm{i}}_{\mathrm{BC}} = \mathrm{AAE}^{\mathrm{i}}_{\mathrm{ff}} = 1$ was set, ~~in-situ AAE for BC by fossil fuel~~ ~~($\mathrm{AAE^i}_{\mathrm{ff,BC}}$)~~ ~~was setto 1,~~ based on the $\mathrm{AAE^i}$ computed over 5 wavelengths at morning rush hour on winter weekdays at UT, consistent with fresh uncoated BC particles (e.g. Liu et al., 2018). ~~No prior information about optical properties of Brown Carbon and biomass burning aerosol in Modena was available, therefore their AAE~~ $\mathrm{AAE^i}$ ~~values were~~ for BrC was determined by a preliminary non-linear fit of Equation 2, performed considering $\mathrm{AAE}^{\mathrm{i}}_{\mathrm{BrC}}$ as a free parameter (and resulting in an average $\mathrm{AAE}^{\mathrm{i}}_{\mathrm{BrC}} = 3.9$); $\mathrm{AAE}^{\mathrm{i}}_{\mathrm{bb}} = 2$ was set based on ~~a preliminary MWAA run and on~~ literature data for the Po valley ~~(Bernardoni et al., 2011, 2013; Vecchi et al., 2018;~~

~~Costabile et al., 2017) : $AAE^{i}_{BrC} = 3.9$ and $AAE^{i}_{bb} = 2$. Asource of uncertainty in this apportionment is the MWAA's omission of absorption by~~ (Bernardoni et al., 2011, 2013; Costabile et al., 2017; Vecchi et al., 2018). A and B were then obtained for each sample by multi-wavelength fit of Equations 2 (after fixing AAE^{i}_{BrC}) and A', B' by multi-wavelength fit of Equations 3. It is noteworthy that the MWAA model neglects possible contributions from mineral dust. To limit ~~this uncertainty~~uncertainties resulting from this, the days with significant dust load were discarded prior the application of the MWAA model to the in-situ data~~.~~, i.e. whenever the in-situ apportionment data is presented throughout the text, it is screened for dust. Days with significant dust content were first identified for the atmospheric column, using the particle volume size distribution estimated by the AERONET inversion (Sinyuk et al., 2020)~~, and subsequently compared with~~; the identification of dust events was performed qualitatively, based on the retrievals having a dominant coarse mode (e.g. Figure S7, panel b). These retrievals were subsequently double-checked by 72-hours HYSPLIT back trajectories using Global Data Assimilation System (GDAS) 1° resolution wind fields. Additionally, the impact of dust at ground ~~levels on these days was evaluated using the daily ratio by~~ level was assessed based on the daily $PM_{2.5}$ to PM_{10} ratio from the in-situ measurements (Figure S1)~~.~~, with ratio ≤ 0.5 as a qualitative threshold for a dust event. For reference, the daily $PM_{2.5}$ to PM_{10} ratio in winter between 2017 to 2021 at the UB site had a median ratio of 0.71 and a 10th (25th) quantile of 0.53 (0.62), i.e. the two aerosol fractions are quite similar, as previously observed at most UB sites across the basin (Bigi and Ghermandi, 2016).

2.4.2 Columnar apportionment

AAOD was apportioned to BC, BrC and mineral dust using the approach proposed in Bahadur et al. (2012), i.e. by directly solving the system of Ångström equations (see Appendix A) using the AERONET almucantar L1.5* retrievals. ~~This~~ The system includes Equation A1, describing the additive contribution of AAOD by each species to the total AAOD and Equation A2, describing the exponential dependence of AAOD on the wavelength. This apportionment method neglects the mixing state of absorbing species (i.e., the aerosol is assumed to be externally mixed), and assumes the observed AAOD is representative of a well-mixed sample of these species. Bahadur et al. (2012) estimated globally valid ranges of AAE^{c} and SAE^{c} for BC, BrC and dust, parameters needed to solve the system of AAE equations, based on long-term, worldwide AERONET observations (version 2, level 2.0).

For the current study, a tailored estimate of the AAE^{c} values for Modena was performed, based on the full time series of AERONET retrievals in Modena (from Jan 2000 to June 2021). The classification of aerosol species (BC, BrC, dust) in order to estimate their AAE^{c} values was performed by combining the approaches by ~~Cazorla et al. (2013), Bahadur et al. (2012)~~ Bahadur et al. (2012), Cazorla et al. (2013) and Shin et al. (2019). Cazorla et al. (2013) suggests threshold values in SAE^{c} and AAE^{c} across the 440 – 675 nm range (hereafter $SAE1^{c}$ and $AAE1^{c}$), which were applied for a preliminary classification (Figure S2). Shin et al. (2019) combined the particle linear depolarization ratio and the lidar ratio at 1020 nm into a dust ratio coefficient $\chi_{d,\lambda}$, estimating the contribution by dust and non-dust aerosol to AOD. Following Bahadur et al. (2012), in order to disentangle the spectral properties of fossil fuel and biomass burning aerosol, first AAE^{c} for dust was assessed using the full L1.5* time series (259 data points), based on the conditions $SAE1^{c} < 1$, $AAE1^{c} > 1.5$ and $\chi_{d,1020nm} > 0.8$. Since the major source of biomass burning in the Po valley is domestic heating during winter. AAE^{c} for BC was estimated based on the full time series of summer L1.5* retrievals (1752 data points)~~, since the major source of biomass burning in the Po valley is domestic heating, during winter; the conditions applied~~. The conditions applied in this case were SAE1^c > 1.2 and AAE2^c/AAE1^c > 0.8, with ~~the index~~ index 1 indicating th range 440 – 675 nm and index 2 indicating the range 675–880 nm (Bahadur et al., 2012). Then the AAE^c for BrC was computed by solving the AAE equations system on the L1.5* non-dust winter retrievals over the period 2015-2022 (89 data points). ~~This procedure provided a median estimate~~ AAE^c for BC and BrC are based on datasets with different size since in winter fewer retrievals are available, due to shorter daytime duration and clouds: to limit the possible bias induced by this difference in sample size and by the potential presence of outliers, the median ± median absolute deviance of the AAE^c for dust, BC and BrC ~~for~~ were computed, for both Modena and Ispra (see below)~~as~~, and reported in Table 1. Table 1 also includes literature values of column AAE^c for different absorbing aerosol types for comparison.

To assess the representativity of the AAE^c values derived for Modena, sun/sky photometer retrievals in Modena were also compared to AERONET data from Ispra (45.80° North, 8.63° East, 220 m a.s.l., 225 km NW of Modena) collected by a second Cimel CE-318 sun/sky photometer within the AERONET network. Ispra exhibited a SAE^c/AAE^c matrix very similar to that observed in Modena (not shown). The resulting AAE^c values for BC, BrC and dust in Modena and Ispra (Table 1) are consistent with most of the existing literature and the variability reported therein ~~(e.g. Bahadur et al., 2012; Giles et al., 2012; Kayetha et al., 2022; Russell et al., 2010)~~(e.g. Russell et al., 2010; Bahadur et al., 2012; Giles et al., 2012; Kayetha et al., 2022) .

Finally, with reasonable confidence in the tailored AAE values for the different absorbing components, each AERONET retrieval at Modena and Ispra was apportioned by summarizing the solutions of the equation system as described by Bahadur et al. (2012). ~~This was done by randomly extracting 10^4 AAE^c samples assuming AAE^c to be normally distributed and with a~~ The apportionment was performed by the following two step procedure, based on the assumption that AAE^c followed a normal distribution featured by the parameters in Table 1.~~The~~

– Step 1. random extraction of AAE^c for all species at all wavelengths

– Step 2. direct solution of the system of Ångström equations

The steps 1 and 2 were repeated 10^4 times for each retrieval in order to develop statistics of the AAE^c combination that provides a solution to the system. The time series of median AAE^c values was fairly stable over the measurement period, at both sites, except during an intense ~~episodes~~ episode of dust transport, when the AAE^c for BrC increased significantly and AAE2^c for dust dropped (Figure S3). Both AAE^c for BrC and AAE2^c for dust values were on the tails of their respective distributions. It is worth noting that AAE^c refers to BC and not to eBC since it proceeds from a direct estimate of the absorption wavelength dependence of aerosol particles while suspended in air.

3 Results

3.1 Diurnal patterns for the in-situ data

Figure 2 shows the medians and interquartile ranges of atmospheric species obtained from in-situ observations along with hourly traffic count from the induction loops closest to each monitoring site for winter (December, January and February) from early 2020 until March ~~2021~~2021. This data is screened for days with non-negligible dust load, as specified in ~~2.1.~~ 2.4.1. The

Table 1. Summary table of columnar Absorption Angstrom Exponent (AAE[c]) for BC, BrC and dust by this work and other literature studies. Rows are organised by wavelength.

Citation	Setting	BC or alike		BrC or alike		Dust	
		Wavelength (nm)	AAE[c]	Wavelength (nm)	AAE[c]	Wavelength (nm)	AAE[c]
This work	AERONET, Modena, Italy	440 – 675	1.12 ± 0.11	440 – 675	4.35 ± 1.28	440 – 675	2.83 ± 0.69
This work	AERONET, ~~Modena~~Ispra, Italy	~~675~~ 440 – ~~870~~ 675	~~1.10~~ 1.11 ± ~~0.11~~ 0.10	~~675~~ 440 – ~~870~~ 675	~~–~~4.33 ± 1.04	~~675~~ 440 – ~~870~~ 675	~~1.06~~ 3.51 ± ~~0.57~~0.97
~~This work~~ Bahadur et al. (2012)	AERONET, ~~Ispra, Italy~~ worldwide	440 – 675	~~1.11~~ 0.55 ± ~~0.10~~ 0.24	440 – 675	~~4.33~~ 4.55 ± ~~1.04~~ 2.01	440 – 675	~~3.51~~ 2.20 ± ~~0.97~~0.50
This work	AERONET, ~~Ispra~~Modena, Italy	675 – 870	~~1.13~~ 1.10 ± ~~0.10~~ 0.11	675 – 870	–	675 – 870	~~0.97~~ 1.06 ± ~~0.56~~0.57
~~Bahadur et al. (2012)~~ This work	AERONET, ~~worldwide~~ Ispra, Italy	~~440 –~~ 675 – 870	~~0.55~~ 1.13 ± ~~0.24~~ 0.10	~~440 –~~ 675 – 870	~~4.55 2.01 440~~ –	675 – 870	~~2.20~~ 0.97 ± ~~0.50~~0.56
Bahadur et al. (2012)	AERONET, worldwide	675 – 870	0.85 ± 0.40	675 – 870	–	675 – 870	1.15 ± 0.50
Dubovik et al. (2002)	AERONET, worldwide	440 – 870	0.4 – 2.5~~*~~[a]			440 – 870	0 – 1.6
Giles et al. (2012)	AERONET, worldwide	440 – 870	1.0 – 1.4			440 – 870	1.5 – 2.3
~~Kayetha et al. (2022)~~ Russell et al. (2010)	~~OMI-MODIS-AERONET~~AERONET, worldwide	~~340~~ 440 – ~~646~~ 870	~~1.0~~ ∼ 0.7 – ~~1.3*~~ 1.2[a]			~~340~~ 440 – ~~646~~ 870	~~2.7~~ ∼ 1.5 – ~~3.8~~2.6
~~Mallet et al. (2013)~~ Zhang et al. (2022)	AERONET~~, Mediterrenean~~ /GRASP[b], worldwide	440 – 870	1.1 – 1.2[a]			440 – 870	∼ ~~1.96[§]~~1.2 – 3
~~Russell et al. (2010)~~ Mallet et al. (2013)	AERONET, ~~worldwide~~ Mediterrenean	~~440 – 870~~	~~∼ 0.7 – 1.2*~~			440 – 870	∼ ~~1.5 – 2.6~~1.96[c]
~~Zhang et al. (2022)~~ Kayetha et al. (2022)	~~AERONET/GRASP°~~OMI-MODIS-AERONET, worldwide	~~440~~ 340 – ~~870~~ 646	~~1.1~~ 1.0 – ~~1.2*~~ 1.3[a]			~~440~~ 340 – ~~870~~ 646	~~∼ 1.2~~ 2.7 – ~~3~~3.8
Zhu et al. (2021)	SKYNET~~#~~[d], Fukue, Japan			340 – 500	5.3		

[a] These values are referred generically to 'urban/industrial/polluted aerosol', i.e. potentially from a mixture of BC and BrC

[b] GRASP: Generalized Retrieval of Aerosol and Surface Properties (Dubovik et al., 2014)

[c] These values are referred generically to 'dusty sites'

[d] SKYNET is a worldwide network of sun/sky photometers (Nakajima et al., 2020)

σ_{ap} at 528 nm for winter weekdays (Monday through Friday) and winter holidays (i.e. Sundays, local and national holidays) is in the top ~~pane~~ panel of Figure 2 and represents the absorption by aerosol at about 4 m above the ground. Saturdays are excluded due to their mixed signal between a holiday and a weekday. The pattern of absorption apportionment components at 880 nm ~~, in days with negligible dust load,~~ is also shown, followed by NO, NO_2, O_3 (UB only) and C_6H_6 (UT only). Figure 3, based on the same dataset as Figure 2, displays the share of σ_{ap} at 375 nm due to BC from fossil fuel, BC from biomass burning and to BrC, along with the variability in AAE over the range 375 – 880 nm. The medians and interquartile ranges for meteorological variables over the same period are shown in Figure ~~S4~~4, while the hourly wind rose is shown in Figure ~~S5~~S4. Overall median and interquartile ranges for ~~weekdays and holidays during the investigated period for atmospheric species and meteorological variables~~ the dataset in Figure 2 (i.e. with dust screening) and Figure 4 are shown in Tables 2 and ~~??~~ S1 respectively.

~~The hourly mean for~~ Table 3 reports a comparison of aerosol and BrC absorption reported by this and other studies at a few Po valley sites. Values in Modena are generally higher than those reported in urban background Milan and the rural background sites of Motta Visconti and Ispra (Ferrero et al., 2021b; Gilardoni et al., 2020a; Laj et al., 2020; Zanatta et al., 2016). The data from these earlier studies comes from filter absorption photometers, either MAAP or aethalometers, with the latter instrument corrected for multiple-scattering-induced bias based on co-located observations. For example in Gilardoni et al. (2020a) a C_{ref} = 3.0 based on Collaud Coen et al. (2010) was used to correct AE22 absorption. Compared to other Southern European urban sites, Modena recorded larger σ_{ap} at ~~880 nm is 22.1 (standard deviation: 15.5) , larger than the mean (standard deviation) levels measured by an Aethalometer AE22 in urban background Milan in winter 2016 (Gilardoni et al., 2020a), which found 12.1 (8.5) , and lower than~~ 660 nm than Barcelona (Ealo et al., 2018), but lower σ_{ap} at ~~880 nm of 31.1 (0.5) also reported in Milan in December by Ferrero et al. (2021b). The mean for σ_{ap} at~~ 375 ~~nm in Modena exhibited even larger values (75.4~~

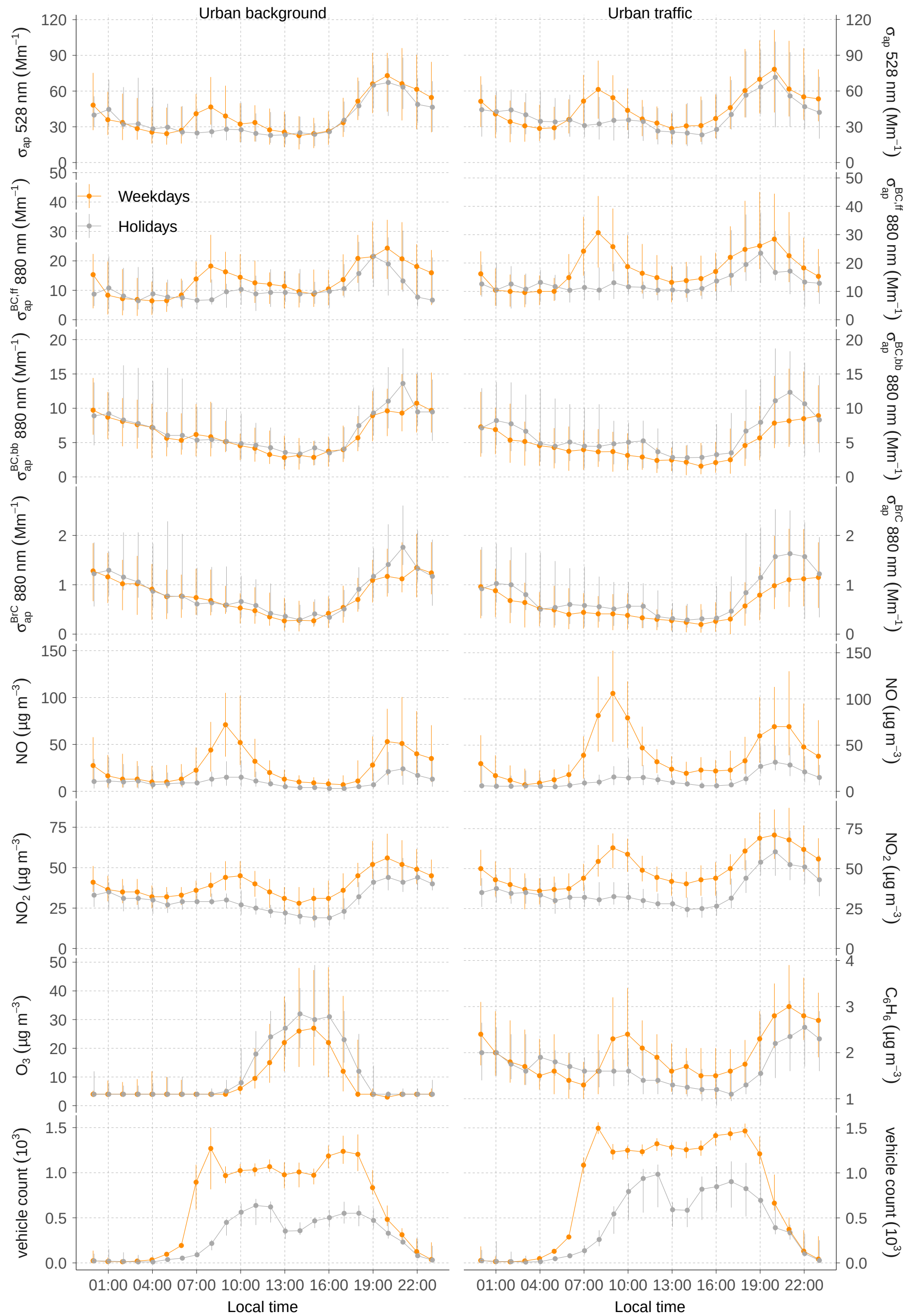

Figure 2. Diurnal pattern for the medians and the interquartile ranges for total $\sigma_{\rm ap}$ at 528 nm, the apportioned $\sigma_{\rm ap}$ at 880 and regulatory gas compounds at the urban background (left) and urban traffic (right) air quality monitoring site, for weekdays (orange) and holidays (grey).

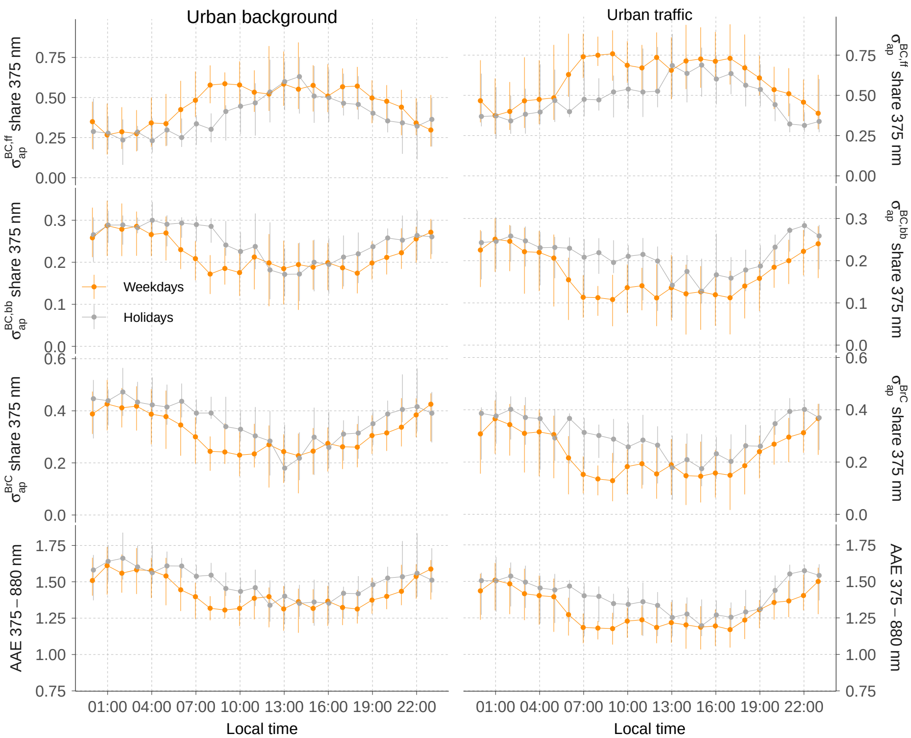

Figure 3. Diurnal pattern for the medians and the interquartile ranges for apportioned σ_{ap} at 375 nm and of the AAE (375 – 880 nm) at the urban background (left) and urban traffic (right) air quality monitoring site, for weekdays (orange) and holidays (grey).

~~, standard deviation: 52.2) than winter 2016 both in Milan, where the mean (standard deviation) was 38.8 (27.6) , and in rural background Po valley (Motta Visconti, Gilardoni et al., 2020a), where the mean (standard deviation) was 28.7 (30.1) . However, mean absorption values in the UV in Modena were lower than the mean (standard deviation)~~ ~~σ_{ap}~~ ~~for this same wavelength in~~ nm than Athens (Greece)~~by AE33 during wintertime, where they found 82.77 (133.3) (Kaskaoutis et al., 2021) .~~, mainly due to the large impact by biomass burning emissions in ~~Athens (Liakakou et al., 2020; Katsanos et al., 2019). Absorption data in Milan urban area and in Athens were corrected for multiple-scattering-induced bias based on co-located MAAP observations, with the data from Milan (measured by an AE22) using a~~ ~~$C_{ref} = 3.0$~~ ~~based on Collaud Coen et al. (2010)~~ this city (Liakakou et al., 2020; Katsanos et al., 2019). A similar pattern is observed for BrC absorption. No MAAP co-location was available for the two MA200s in Modena, leading to a larger uncertainty in their absolute readings; however these two units showed ~~a large agreement with~~ good agreement with a MAAP during a BC intercomparison in urban background Athens (Stavroulas et al., 2022), where they exhibited a linear slope of 1.00 (R^2 = 0.92) in winter and 1.07 (R^2 = 0.92) in summer. ~~Geometric mean of daily absorption at 625 nm in Modena was 28.7 , almost 50% higher than the absorption in Ispra obtained from a MAAP for winter 2008–2011, where daily geometric mean (geometric standard deviation) resulted 18.6 (1.72) (Zanatta et al., 2016). The winter hourly mean absorption at 528 nm in Modena, of 43.8 , is consistently more than twofold~~

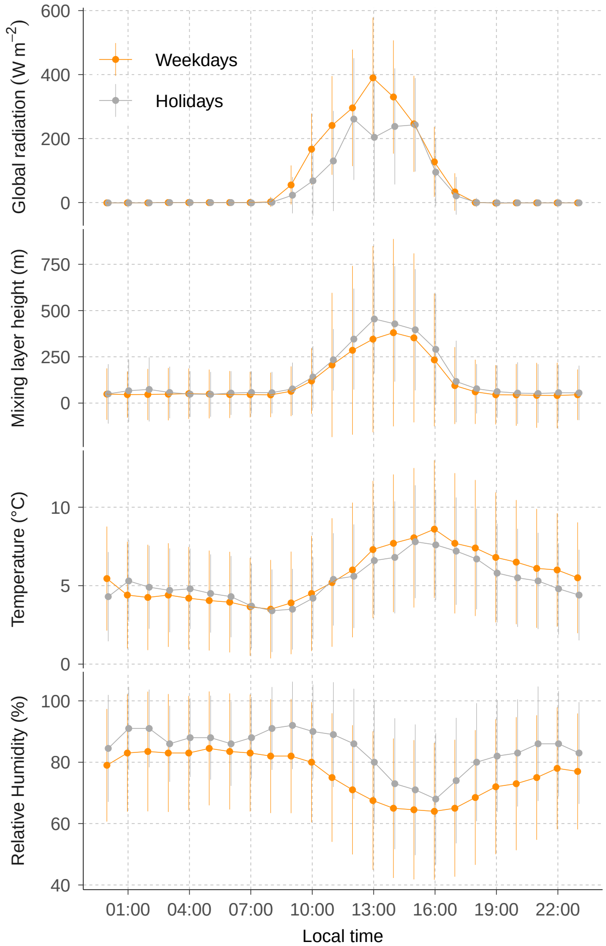

Figure 4. Diurnal pattern for the medians and the interquartile ranges of meteorological variables in winter (DJF) during weekdays and holidays All variables proceed from an urban meteorological station, besides mixing layer height, provided by ERA5 reanalysis.

~~larger than the hourly median σ_{ap} in Ispra by AE31 during winter 2016 (Laj et al., 2020), which was 17.3 . Also the daily mean (standard deviation) UV (375 nm) absorption by BrC in Modena (25.9 (13.7)) is higher than the daily mean (standard deviation) of BrC measured by an AE22 in urban Milan and the rural background Po valley (Gilardoni et al., 2020a) in winter 2016, which were 10.8 (4.9) and 9.5 (5.4) respectively. Similar to BC, the mean BrC levels in Modena are lower than the wintertime mean in Athens (36.73–73.63 reported by Kaskaoutis et al. (2021)).~~

The diurnal pattern for absolute levels of fossil fuel combustion species (Figure 2) exhibits a similar pattern. There is an initial increase during the morning rush hour (8:00 to 10:00 Local Time, LT), followed by a drop at midday due to the dilution induced by an increased MLH depth despite the steady traffic rate. A second increase occurs at 18:00 LT followed by a drop ~~since ca.~~ at approximately 20:00 LT, delayed compared to the drop in traffic, possibly because of the shallow MLH in the evening or because of frequent thermal inversions at ground level. More specifically, on weekday evenings $\sigma_{\mathrm{ap}}^{\mathrm{BC,ff}}$ peaks at

Table 2. Summary table of atmospheric species and traffic volume for the UB and the UT site.

Variable	Urban background						Urban traffic					
	Weekdays			Holidays			Weekdays			Holidays		
	med	25th q	75th q	med	25th q	75th q	med	25th q	75th q	med	25th q	75th q
σ_{ap} 528 nm (Mm^{-1})	~~37.2~~ 37.1	~~20.8~~ 20.5	~~63.8~~ 63.0	~~31.9~~ 32.3	~~21.8~~ 21.4	~~61.8~~ 63.9	42.4	~~24.5~~ 24.8	~~70.4~~ 69.1	~~39.6~~ 38.1	~~22.6~~ 21.6	~~60.2~~62.7
$\sigma_{ap}^{BC,ff}$ ~~IR~~ 880 nm (Mm^{-1})	~~11.5~~ 12.6	~~5.0~~ 5.5	~~21.2~~ 22.2	~~9.1~~ 9.6	~~4.3~~ 4.6	~~20.0~~ 19.0	~~16.8~~ 16.9	~~9.0~~ 9.1	~~27.9~~ 28.1	~~12.8~~ 12.7	~~7.6~~ 7.0	~~19.7~~20.6
$\sigma_{ap}^{BC,\,bb}$ ~~IR~~ 880 nm (Mm^{-1})	~~5.9~~ 6.1	~~3.0~~ 3.1	~~10.5~~ 10.6	~~6.2~~ 6.3	~~4.1~~ 3.7	~~9.6~~ 12.0	4.3	1.4	8.8	~~5.2~~ 5.1	~~2.5~~ 2.3	~~11.2~~11.1
σ_{ap}^{BrC} ~~IR~~ 880 nm (Mm^{-1})	0.8	0.3	1.4	0.8	0.4	~~1.4~~ 1.5	0.5	0.1	1.1	0.7	~~0.3~~ 0.2	1.5
NO ($\mu g\,m^{-3}$)	~~19~~ 20	6	~~48~~ 49	8	4	~~20~~ 21	~~29~~ 31	~~11~~ 12	~~63~~ 64	~~12~~ 10	5	~~27~~25
NO_2 ($\mu g\,m^{-3}$)	~~38~~ 39	29	48	29	21	38	~~47~~ 48	~~36~~ 37	~~60~~ 61	~~35~~ 34	~~26~~ 25	~~48~~46
O_3 ($\mu g\,m^{-3}$)	5	4	16	~~8~~ 7	4	24	–	–	–	–	–	–
C_6H_6 ($\mu g\,m^{-3}$)	–	–	–	–	–	–	1.9	1.3	2.7	1.6	~~1.3~~ 1.1	2.3
~~vehicle count~~ vehicles per day (10^3)	~~673~~ 16.1	~~92~~ 14.3	~~1073~~ 31.9	~~286~~ 7.2	~~72~~ 5.9	~~490~~ 9.1	~~938~~ 19.9	~~118~~ 17.2	~~1303~~ 38.0	~~372~~ 11.3	~~86~~ 7.7	~~735~~13.9

20:00 LT, one hour later than on holidays, at both UB and UT~~.~~, with the former site recording $\sigma_{ap}^{BC,ff}$ levels higher in the evening than in the morning.

This main pattern is followed by all atmospheric species except for secondary pollutants (e.g. O_3) and aerosols related to biomass burning (e.g. $\sigma_{ap}^{BC,bb}$ and σ_{ap}^{BrC}). The pattern features higher concentrations during weekdays than holidays at both sites, as shown by the 7% – 240% increase on weekdays, similar to the 230% – 250% increase in traffic, confirming a major and local fossil fuel combustion direct origin. For most of these species the absolute interquartile range (IQR) is larger on weekdays than holidays. For gas phase compounds the IQR increased on weekdays from 8% for NO_2 at UT to 160% for NO at the UB. For absorption the largest increase in IQR (a 56% increase) occurred for $\sigma_{ap}^{BC,ff}$ at the UT. The difference in variability between weekdays and holidays might be partly driven by the larger variability in fossil fuel combustion emissions during the former, along with the larger count of weekdays compared to holidays in the statistics.

$\sigma_{ap}^{BC,bb}$ and σ_{ap}^{BrC} ~~show~~ exhibit a diurnal pattern ~~featured by~~ featuring an increase from 17:00 LT to 23:00 LT possibly triggered by the decrease in both the MLH and T, leading to condensation of semivolatile organics and to an increase in biomass burning emissions. A similar diurnal pattern for BrC absorption was observed in UB Milan and rural background Po valley (Gilardoni et al., 2020a), and in UB Athens ~~(Kaskaoutis et al., 2021; Liakakou et al., 2020)~~(Liakakou et al., 2020; Kaskaoutis et al., 2021). The weekly pattern for these two species is larger at the UT, with an increase during holidays in the overall median values of $\sigma_{ap}^{BC,bb}$ and σ_{ap}^{BrC} of 22% and 35% respectively, along with an increase in their IQR of 16% and 28%.

The share of absorption at 375 nm ~~by~~ for the three apportioned species (Figure 3) shows a distinct diurnal and weekly pattern at the UT, with $\sigma_{ap}^{BC,bb}$ and σ_{ap}^{BrC} being ca. 37% larger during holidays, in contrast to $\sigma_{ap}^{BC,ff}$ which is 32% larger on weekdays. ~~A similar patternoccurred~~The UB exhibited a similar pattern, although with lower intensity~~, at the UB~~. The holiday increase in biomass burning aerosol is probably linked to the longer stay at home compared to weekdays and to a large recreational use of biomass burning in town, where most ~~of~~ houses use compressed natural gas for domestic heating and cooking (99.4% of PM_{10} emissions by SNAP 2 in Modena are from biomass combustion for domestic heating according to ARPAE (2020)). The diurnal pattern of the share of absorption by $\sigma_{ap}^{BC,ff}$ at 375 nm is similar to the diurnal traffic count cycle, exhibiting larger

Table 3. Summary table of ~~meteorological variables in Modena during the investigated period~~mean ± standard deviation of absorption for aerosol and BrC based on this work and other literature studies. Rows are organised by wavelength. UB, UT and RB stand for Urban Background, Urban Traffic and Rural Background respectively.

~~Variable~~ Citation	Setting	Period	Wavelength	Absorption
	~~med~~	~~25th q~~	~~75th q~~ (nm)	~~med~~ (Mm^{-1})
	~~25th q~~	~~75th q~~		Aerosol
~~Mixing layer height~~				
This work	~~81~~ MA200, UB, Modena, Italy	~~38~~ winter 2019 – 2021	~~248~~ 880	~~125~~ 22.1 ± 15.5
This work	~~41~~ MA200, UT, Modena, Italy	~~265~~winter 2019 – 2021	880	27.3 ± 21.0
~~Global downward radiation (~~Gilardoni et al. (2020a)	AE22, UB, Milan, Italy	winter 2015 – 2016	880	12.1 ± 8.5
Gilardoni et al. (2020a)	AE22, RB, Motta Visconti, Italy	winter 2015 – 2016	880	7.6 ± 7.1
Ferrero et al. (2021b)	AE31, UB, Milan, Italy	December 2015	880	31.1 ± 0.5[a]
This work	MA200, UB, Modena, Italy	winter 2019 – 2021	375	75.4 ± 52.2
This work	MA200, UT, Modena, Italy	winter 2019 – 2021	375	84.7 ± 67.7
Gilardoni et al. (2020a)	AE22, UB, Milan, Italy	winter 2015 – 2016	370	38.8 ± 27.6
Gilardoni et al. (2020a)	AE22, RB, Motta Visconti, Italy	winter 2015 – 2016	370	28.7 ± 30.1
Kaskaoutis et al. (2021)	AE33, UB, Athens, Greece	winter 2016 – 2017	370	82.8 ± 133.3
This work	MA200, UB, Modena, Italy	winter 2019 – 2021	625	25.1 ± 2.4[b]
This work	MA200, UT, Modena, Italy	winter 2019 – 2021	625	30.3 ± 2.4[b]
Zanatta et al. (2016)	MAAP, RB, Ispra, Italy	winter 2008 – 2011	637	18.6 ± 1.7[b]
Ealo et al. (2018)	MAAP, UB, Barcelona, Italy	winter 2009 – 2014	637	~ 17.4
This work	MA200, UB, Modena, Italy	winter 2019 – 2021	625	28.1 (8.1 – 69.2)[c]
This work	MA200, UT, Modena, Italy	winter 2019 – 2021	625	33.3 (10.0 – 80.3)[c]
Laj et al. (2020)	~~1~~ AE31, RB, Ispra, Italy	~~-1~~ winter 2016	~~87~~ 660	~~1~~ 17.3 (2.5 – 48.2)[c]
	~~-1~~	~~67~~		BrC
~~Relative humidity (%)~~				
This work	~~77~~ MA200, UB, Modena, Italy	~~60~~ winter 2019 – 2021	~~90~~ 375	~~83~~ 26.6 ± 22.2
This work	~~66~~ MA200, UT, Modena, Italy	~~94~~ winter 2019 – 2021	375	23.9 ± 24.2
~~Mean atmospheric temperature (°C)~~Gilardoni et al. (2020a)	~~5.6~~ AE22, UB, Milan, Italy	~~3.1~~ winter 2015 – 2016	~~8.4~~ 370	~~5.4~~ 6.0 ± 2.7[d]
Gilardoni et al. (2020a)	~~3.5~~ AE22, RB, Motta Visconti, Italy	~~7.7~~winter 2015 – 2016	370	5.3 ± 3.0[d]
Kaskaoutis et al. (2021)	AE33, UB, Athens, Greece	winter 2016 – 2017	370	36.7 ± 73.6

[a] 95% confidence interval of the mean

[b] geometric mean ± geometric standard deviation

[c] median (10th - 90th quantile)

[d] BrC determined on methanol extraction

values during weekdays and at the UT. This supports the results of the apportionment and the hypothesis of the role of the MLH in the evening ~~levels~~ enhancement of absorption.

O_3 exhibits a 'weekend effect' (Cleveland et al., 1974), common to most urban areas in Europe having a VOC–limited regime, i.e. ~~with large / VOC ratios for the ozone cycle kinetics (?). On weekdays ozone decreases after 16:00 LT due to the slowdown of the photochemical activity, the oxidation by of and to and respectively. In contrast to weekdays,~~ on holidays ozone rises earlier in the morning due to the lower NO_x levels, leading to a more efficient photocatalytic cycle, and drops later in the evening due to the (later) increase in NO_x~~, as commonly seen in VOC–limited regimes.~~ .

Atmospheric heating by aerosols based on σ_{ap} values in Modena was estimated by determining the HR from AERONET data as detailed in section 2.2. Figure 5a shows the complete HR time series obtained over Modena during the investigated period. Under an average (standard deviation) irradiance value of 386 (143) $\mathrm{W\,m^{-2}}$ the average (standard deviation) HR was 1.61 (1.58) $\mathrm{K\,d^{-1}}$. This value is consistent with data from Milan for wintertime, under clear sky conditions, where a mean (± mean confidence interval) of 1.68 ± 0.04 $\mathrm{K\,d^{-1}}$ was found, when ~~also~~ the incoming radiation was similar (441 ± 148 $\mathrm{W\,m^{-2}}$). This latter is an important point since AERONET data is mainly available under clear sky conditions and thus the obtained HR data represents the upper limit for the site. In the Po valley the HR was shown to decrease by a ∼12% factor for every okta of sky covered by clouds (Ferrero et al., 2021b). With respect to the HR diurnal pattern, Figure 5b shows the mean diurnal pattern of irradiance and HR under clear sky and cloudy conditions. The incoming radiation peaked at 13:00 LT with 529 ± 55 $\mathrm{W\,m^{-2}}$ (Figure 5b) while σ_{ap} peaked between 8:00 and 10:00 LT (Figure 2). This ~~caused~~ causes an asymmetric HR diurnal pattern, characterized by a fast increase to the maximum at 11:00 LT (1.83 ± 0.84 $\mathrm{K\,d^{-1}}$) and a subsequent slower decrease till sunset (Figure 5b), as is common under clear sky conditions ~~(Ferrero et al., 2021b, 2018)~~(Ferrero et al., 2018, 2021b).

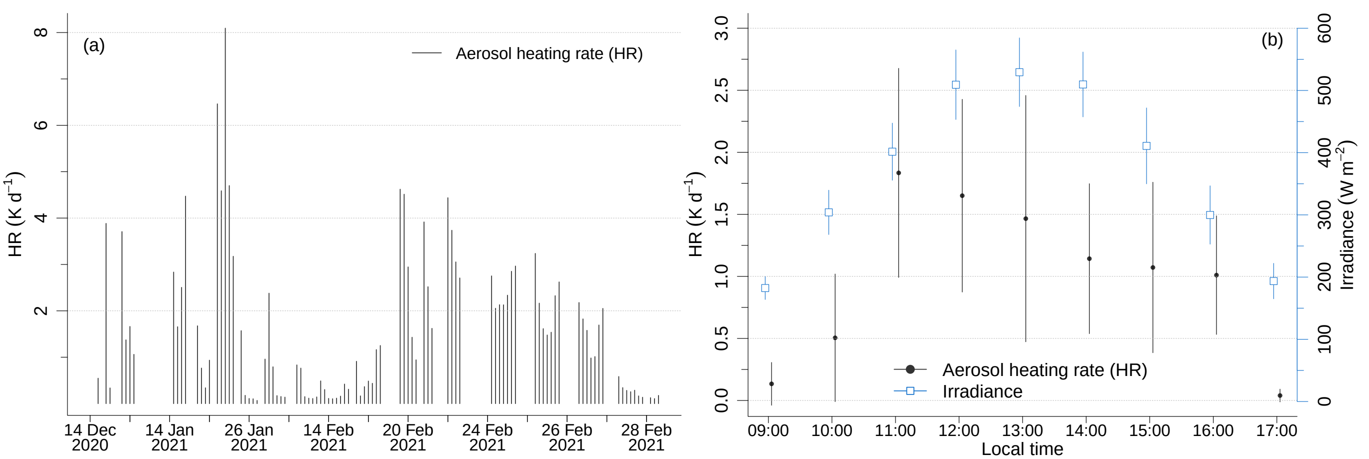

Figure 5. Time series (a) and diurnal pattern (b) of aerosol heating rate (HR) at Modena by AERONET retrievals.

The wind pattern in Modena features a mild mountain-valley breeze system along the Po valley longitudinal axis, ~~super-imposed on a~~ superimposed on the local wind circulation. During the investigated winter period, calm wind conditions (speed lower than 1 $\mathrm{m\,s^{-1}}$) occurred 25% of the time and an overall wind speed average of ca. 1.5 $\mathrm{m\,s^{-1}}$ was recorded. NW winds, blowing from the higher side of the valley, dominated during daytime hours (11:00 - 17:00 LT) and were associated with the highest windspeed (occasionally above 9 $\mathrm{m\,s^{-1}}$). The rest of the day features local W-SW low winds (windspeeds lower than 3 $\mathrm{m\,s^{-1}}$) and some easterly winds (Figure ~~S5~~S4).

A conditional bivariate polar function was applied to NO_x, $\sigma_{ap}^{BC,ff}$ at 880 nm and σ_{ap}^{BrC} at 375 nm at both the UT and UB sites, to identify the position of potential emission sources (Figure 6) on weekdays and holidays, excluding days with significant dust load at ground. Wind speed and direction data were combined with atmospheric compounds levels by the use of conditional bivariate polar functions (Uria-Tellaetxe and Carslaw, 2014), as implemented in the R-software package Openair (Carslaw and Ropkins, 2012). This tool provides information on both the direction and the distance of the (relatively local) emission sources which are contributing significantly to the observed concentration levels, as well as on the wind direction sectors which might provide clean air masses.

At the UB, NO_x and absorption exhibit slightly different directional patterns: both show an increase associated with slow S–SW winds, particularly on weekdays, while $\sigma_{ap}^{BC,ff}$ exhibits an increase on weekdays during NE moderate winds, probably linked to traffic on the busy road 400 m in that direction. σ_{ap}^{BrC} exhibits larger values during holidays during southerly winds, which is different than the pattern for BC from fossil fuels and NO_x for the same period. At the UT site the directional pattern between NO_x and $\sigma_{ap}^{BC,ff}$ are quite similar, highlighting the role of nearby traffic during weekdays and of the major east–west road south of the UT site which contributes mainly during holidays. Also at the UT σ_{ap}^{BrC} is higher during holidays and under southerly winds. This latter increase occurs during evening/night hours (not shown), consistent with biomass burning from domestic heating for recreational use, with the increase probably enhanced by nighttime atmospheric stagnation. Finally, NW moderate winds are associated with low levels in NO_x, $\sigma_{ap}^{BC,ff}$ and σ_{ap}^{BrC}, mainly because NW winds occur primarily at midday during maximum atmospheric mixing.

3.2 ~~In-situ based vs columnar-data based~~ Comparing absorption optical depth from remote sensing and in situ values

In-situ and columnar aerosol optical properties were compared to assess both how representative the surface in-situ aerosol optical measurements are of the mixed layer, and how the absorption within the MLH compares to the atmospheric column. Urban in-situ and column data ~~were~~ was compared over the whole time period, although simultaneous observations were mainly available only in February 2021. For this comparison the in-situ σ_{ap} were rescaled over (i.e. multiplied by) the MLH height, resulting in an estimate of the integral aerosol absorption over the MLH height ~~in~~ representing the case of vertically homogenous σ_{ap} from the ground to the top of this atmospheric layer. The in-situ σ_{ap} in the IR spectral range (λ = 880 nm) rescaled over the MLH height was generally larger than AAOD (Figure 7), for both the L1.5* and L2.0 AERONET inversions, with ~~a mean normalised error~~ mean normalised errors of $\mathrm{MNE} = 2.2$ and $\mathrm{MNE} = 1.7$ respectively. A better agreement occurred for blue wavelengths (λ = 470 nm and 440 nm for the in-situ and the columnar observations respectively) with $\mathrm{MNE} = 1.0$ and $\mathrm{MNE} = 0.8$ for L1.5* and L2.0 respectively. These results suggests an inhomogeneous vertical distribution of aerosols, i.e. most likely the occurrence of a very large accumulation of aerosols at the ground layer if compared to the atmospheric column and to the MLH, similar to previous observations in Milan during very stable atmospheric conditions (Ferrero et al., 2011). The ~~overestimate of scaled~~ overestimation of scaled in-situ aerosol properties compared to columnar aerosol properties observed in this study may be affected by ~~few~~ some concurrent conditions: (a) the large role of traffic and of other ground emissions on aerosol absorption (b) a persistent ground thermal inversion occasionally as low as few hundred meters, according to radiosoundings at 12 UTC ~~in~~ at the rural Po valley site of San Pietro Capofiume (c) a bias in the ERA5 estimate of the MLH. These

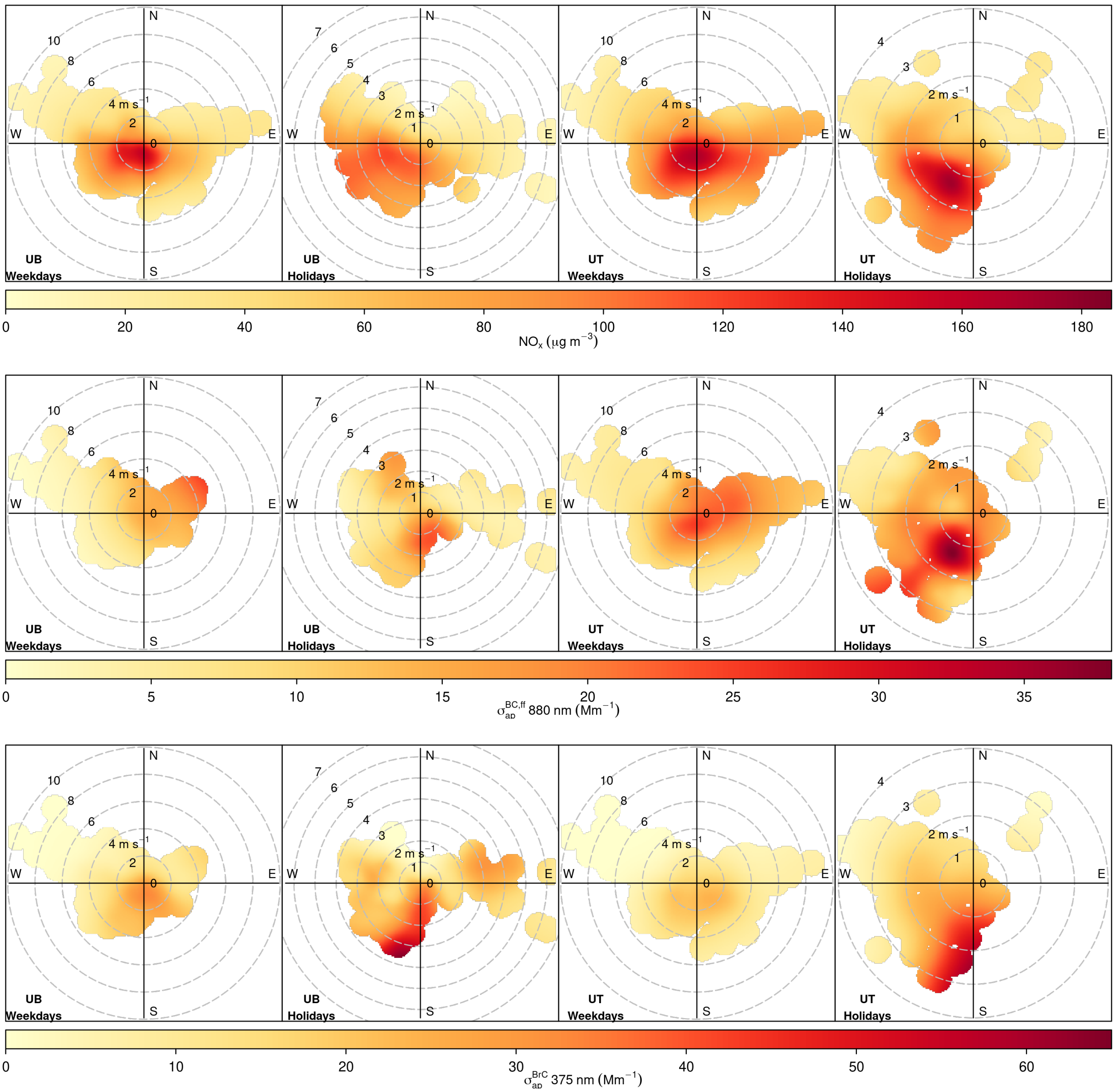

Figure 6. Bivariate polar function applied to NO_x (first row), $\sigma_{ap}^{BC,ff}$ at 880 nm (second row), σ_{ap}^{BrC} at 375 nm (third row) at the UB and UT sites, for weekdays and holidays.

conditions mainly contribute to the significantly larger values observed in scaled ground absorption, particularly at 880 nm, where fossil fuel emissions provide the largest ~~contribute. Consistently, at~~ contribution. At remote sites an opposite pattern was ~~found in the literature (e.g. Bergin et al., 2000; Aryal et al., 2014; Chauvigné et al., 2016; Slater and Dibb, 2004)~~consistently found (e.g. Bergin et al., 2000; Slater and Dibb, 2004; Aryal et al., 2014; Chauvigné et al., 2016), where MLH-scaled surface in-situ atmospheric extinction underestimates sun photometry observations of AOD, mainly because of aerosol ~~hygroscopcity~~ hygroscopicity (in-situ measurements are typically made at low RH) and ~~of~~ aerosol layers above the MLH.

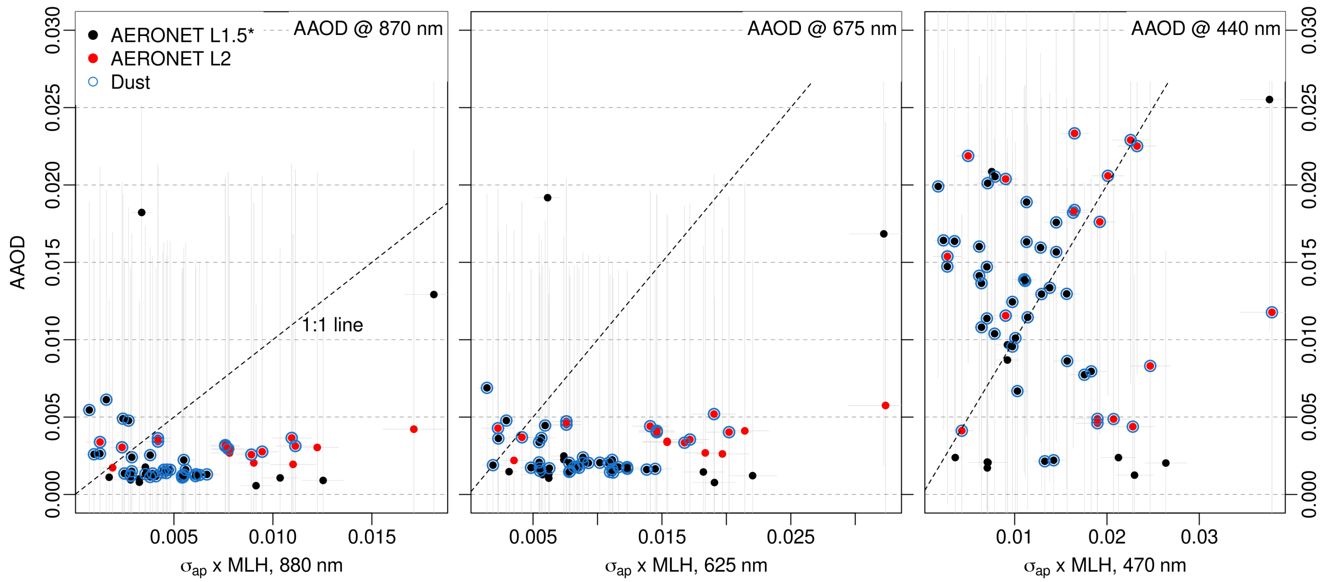

Figure 7. Absorption aerosol optical depth based on columnar and in-situ observations in the IR (left), Green (centre) and UV (right) regions, using both L1.5 and L2.0 AERONET retrievals. Bars indicate measurement uncertainty.

For an assessment of the role of the MLH and of atmospheric layers in the discrepancies between surface and column observations mentioned above, an analysis of the Apparent Aerosol Optical ~~Depth (ApAOD~~Height (ApAOH) was performed. ~~ApAOD~~ ApAOH can be defined as the ratio between AAOD and σ_{ap} (giving ApAOH units of length) to represent the atmospheric depth below which aerosols are uniformly distributed (Loía-Salazar et al., 2014). In the case of well-mixed conditions for absorbing aerosols, ~~ApAOD~~ ApAOH is similar to the MLH, while larger differences indicate less vertical mixing of the aerosol particles.

The comparison of ~~ApAOD~~ ApAOH using L1.5* and MLH in Figure 8a shows how ~~ApAOD ison average lower than~~ ApAOH is, on average, lower than the MLH, at both 880 (870) nm (Mean Error ME $= -243$ m) and 470 (440) nm (ME $= -96$ m) wavelengths of the in-situ (columnar) instruments. In the period February 22nd - 26th ~~ApAOD was~~ ApAOH was highly consistent with the MLH for 470 (440) nm ~~(~~showing a ME $= 31$ m~~), but lower~~ , i.e. similar to the bias reported for ERA5 estimates of MLH in Europe by Guo et al. (2021). Conversely ApAOH at 880 (870) nm was significantly lower than MLH (ME $= -190$ m), suggesting a different vertical mixing between two absorbing aerosol species. The end of February 2021 featured the development of a strong anticyclone system in the Mediterranean basin, leading to above-average atmospheric temperature in Southern and Central Europe, clear sky (as shown by the high frequency of retrievals), the build-up of atmospheric pollutants and the arrival in Italy of Saharan dust rich air masses. During the development of this high pressure system, daily soundings collected at 00 UTC and 12 UTC at the rural site of San Pietro Capofiume (44.65° N, 11.62° E, 60 km east of

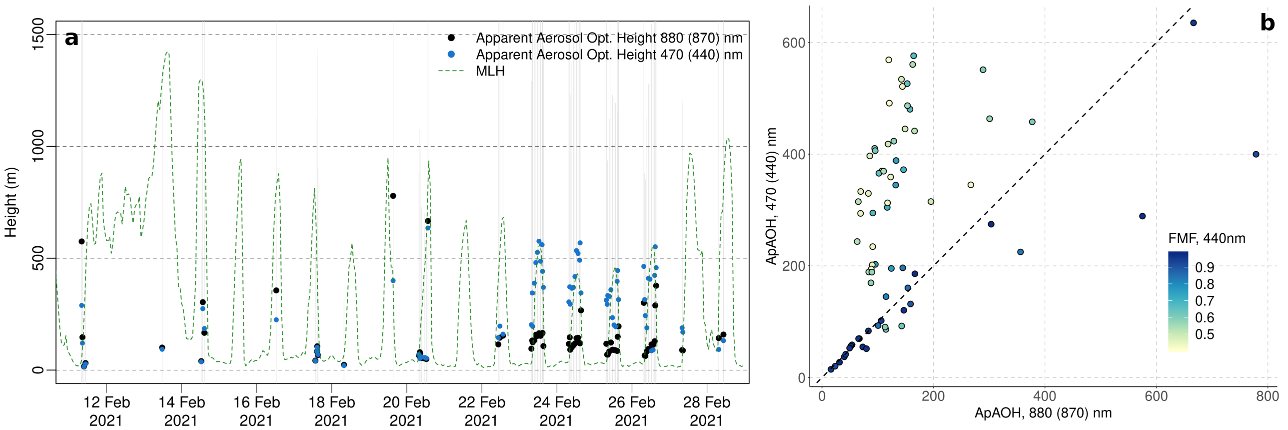

Figure 8. a: Apparent aerosol optical ~~depth~~ height (ApAOH) computed based on aerosol absorption at 880 nm (870 nm) and 470 nm (440 nm) by in-situ (columnar, L1.5*) instruments. Simulated MLH depth by ERA5 is also plotted. b: ~~Apparent aerosol optical depth (ApAOD)~~ ApAOH computed based on aerosol absorption at 880 nm (870 nm) and 470 nm (440 nm) by in-situ (columnar) instruments and color-coded according to the Fine Mode Fraction (FMF) at 440 nm. The dashed line indicates the 1:1 line.

Modena) show the progressive vertical drop of a thermal inversion from ca. 2km (on Feb 20th) to ca. few hundred meters (on Feb 26th), leading to above seasonal median levels for the in-situ σ_{ap} at both 880 nm and 470 nm (Figure ~~S7~~S6). Concurrent AAOD observations were above the median at 440 nm and within the seasonal median at 870 nm, leading to different ~~ApAOD~~ ApAOH values for these two wavelengths (Figure 8a). Differences in AAOD might originate from a different atmospheric layering and mixing of aerosols species: the volume size distribution from the AERONET inversion shows a switch from a major modal peak in submicron diameters on February 20th (Figure ~~S8a~~S7a) to a modal peak in the supermicron diameter range on February 23rd (Figure ~~S8b~~S7b), which lasted until February 27th at midday. Consistently AOD at 500 nm derived by the AERONET Spectral De-Convolution Algorithm (Sinyuk et al., 2020) had a monthly minimum during this clear sky period, showing a switch from a fine aerosol controlled AOD (until Feb 20th) to a coarse aerosol controlled AOD (since Feb 23rd). This suggests that ~~ApAOD in Blue~~ ApAOH at 470 (440) nm is similar to the MLH depth most likely because of a good vertical mixing of dust aerosol, as shown by the decrease in $\mathrm{PM}_{2.5}$ / PM_{10} ratio over the same period (Figure S1), while the low ~~ApAOD~~ ApAOH in the IR is probably due to the dominant contribution of (~~low-height~~ground level) traffic emissions to the σ_{ap} ~~in~~ at this latter wavelength~~, suggesting~~. This suggests that, in this case, the radiative effect by traffic emissions was relevant mainly at the urban scale. ~~Consistently~~ Figure 8b shows how ~~ApAOD~~ ApAOH at 880 (870) nm and 470 (440) nm are correlated and mainly lay on the 1:1 line during high FMF_{440} conditions and aerosol volume size distribution with a fine mode peak (Figure ~~S8a):~~ S7a). For $\mathrm{FMF}_{440} > 0.8$, linear Pearson's correlation $r = 0.91$, with FMF_{440} indicating the contribution by fine aerosol to AOD in the Blue range, where dust is a significant absorber. During low FMF_{440} the ~~ApAOD~~ ApAOH at 470 (440) nm increases significantly, ~~contrarily to ApAOD~~ in contrast to ApAOH at 880 (870), nonetheless the correlation between the two remains.

3.3 Comparison of the contribution by BrC to absorption based on in-situ and columnar data

The contribution of BrC to absorption in Modena according to the in-situ and to the columnar L1.5* data was also compared (Figure 9). Days with significant dust load were removed from the comparison, because the MWAA apportionment method does not include dust absorption~~,~~. This is necessary since, as shown by the ~~ApAOD~~ApAOH, the vertical mixing of dust can be significant, affecting both columnar and in-situ observations. Figure 9 compares the contribution of biomass burning to absorption in Blue (470 nm and 440 nm for the columnar and in-situ observations respectively) by the two apportionment models for 17 matched data points. Calculated statistics indicate a $\mathrm{ME} = 0.04$, a $\mathrm{MNE} = 1.23$ and low linear correlation (Pearson's $r = 0.39$, Spearman's $\rho = 0.34$). According to columnar retrievals the biomass burning contribution ranged between 2% and 23%, with a median (median absolute ~~deviance~~deviation) of 3.9% (0.8%) and a mean (standard deviation) of 5.3% (4.3%); in-situ observations exhibited a similar range ($0\% - 24\%$), but suggested a higher contribution of biomass related to lower MLH depth and a median (median absolute ~~deviance~~deviation) of 8.7% (8.7%). Despite the uncertainty associated with these estimates, these results highlight how urban BrC emissions have a ~~larger~~ large impact on the lower levels of the atmosphere, similar to the findings by Ferrero et al. (2011) for BC. This is consistent with the dynamics of biomass burning emissions from domestic heating, featuring a low exit velocity and negligible plume rise, particularly for natural convection fireplaces or traditional wood-stoves. This BrC absorption contribution is based on days with negligible dust content and thus represents a higher end estimate; nonetheless it is lower than values found for polluted urban sites in ~~East~~ eastern Asia, e.g. Beijing, Hong Kong, Seoul, and Osaka, where the share of AAOD due to BrC ranged between $12\% - 14\%$ in the UV during non-dust days on a yearly basis (Cho et al., 2019). Even larger contributions than those found for the ~~East-Asian~~ eastern Asian sites were reported for Europe during winter where a mean 21% of AAOD in Blue by BrC was reported by Wang et al. (2016b), based on 10 years (2005 – 2014) of AERONET data, also excluding 'dust days'. It is worth noting that over the same decade, Wang et al. (2016b) also reported the in-situ mean share of absorption by BrC in winter at Ispra and SIRTA (Paris, France) to be $\sim$23%. A similar study in California found that the contribution by BC and BrC to absorption by in-situ and ground based sun/sky photometer can be similar, depending on the vertical mixing of the planetary boundary layer ~~Chen et al. (2019)~~ (Chen et al., 2019). They showed according to both methods, the share of BrC absorption at 440 nm was approximately 30%. Similarly, during high pollution events in the Kathmandu valley, Kim et al. (2021) found a good correlation between the in-situ and the columnar estimate of BC and BrC. They estimated a similar share of UV absorption by BrC: 34% and 31% by Aethalometer AE33 and AERONET, respectively and a good ~~linear regression agreement~~ correlation between the two techniques ($R^2 = 0.71$).

3.4 Spatial variability of ground-based columnar retrievals

In addition to checking the vertical mixing of aerosol, spatial mixing in ground-based columnar properties across part of the Po valley during the studied period was also investigated by comparing AERONET L1.5* version 3 retrievals in Modena and Ispra. The observations from the two instruments were matched when collected within the same hour. The AOD data are partly scattered along the 1:1 line (Figure 10), with a significant (at the 95%) Pearson's (Spearman's) correlation coefficient ranging

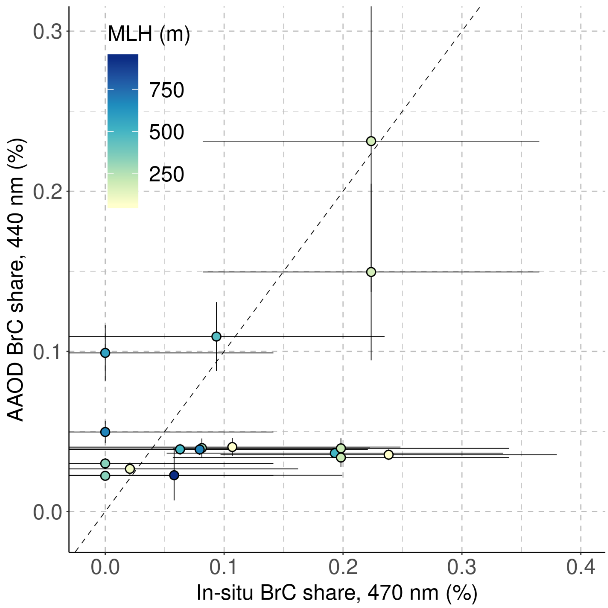

Figure 9. Scatter plot of the share of total AAOD due to BrC and the share total in-situ absorption due to BrC. Bars indicate measurement uncertainty.

from $r = 0.67$ ($\rho = 0.56$) at 440 nm, to $r = 0.84$ ($\rho = 0.79$) at 1020 nm and an orthogonal regression coefficient ranging between 0.74 at 440 nm and 1.4 at 1020 nm. The high correlation in the AOD at the two sites is mainly driven by the observations in February, when both sites experienced a drop in FMF and an increase in AOD because of the dust transport event. This dust event was also detected in Ispra by a ground-based LIDAR within the EARLINET network, whose total attenuated backscatter at 500 and 1064 nm showed an aerosol layer between 1.3 – 2.3 km above the ground during February 23 and 24. The layer subsequently dropped to heights between few hundred meters and 1.8 km on February 25 (no LIDAR data is available for February 26th and 27th). The temporal variability in AOD_{440} and FMF_{440} between the two sites also shows a similar pattern (Figure 10). AOD in Ispra was similar to Modena for most retrievals, with ~~the Ispra and the~~ Ispra and Modena having overall median AOD_{500} values of 0.27 and 0.24 respectively. The two sites differed during mid January, when Modena had median $AOD_{500} = 0.21$, while Ispra had a median $AOD_{500} = 0.12$, consistent with Modena being a site more representative of urban pollution than Ispra.

Concurrent AAOD retrievals at two sites have a different correlation pattern than AOD (Figure ~~S9~~S8), exhibiting the largest linear correlation at 440 nm ($r = 0.70$, $\rho = 0.72$, both statistically significant at the 95% level). The correlation decreases noticeably with increasing wavelength: for 675 nm ($r = 0.42$, $\rho = 0.43$, 95% significance) and 870 nm ($r = 0.37$, $\rho = 0.40$, 95% significance), while no significant correlation occurred at 1020 nm. In contrast to AOD, AAOD at Ispra was larger than at Modena, with median $AAOD_{440}$ being 0.025 and 0.011 ~~at Ispra and the~~ in Ispra and Modena, respectively. The differences in AAOD at the two sites decreased at longer wavelengths, with median $AAOD_{870}$ being 0.003 and 0.002 in Ispra and Modena respectively. According to the apportionment model (Figure ~~S6~~S5) the larger AAOD~~in Blue~~ $_{440}$ at Ispra is due to a larger impact by dust at this site compared to Modena, with $AAOD_{440,dust}$ being 0.022 and 0.001 at the two sites respectively. $AAOD_{440,dust}$ was the component with the largest correlation between the two sites (r = 0.62, ρ = 0.60, 95% significance), followed by BC (r = 0.50, ρ = 0.43, 95% significance), with similar correlation values for $AAOD_{870,dust}$ and $AAOD_{870,BC}$ for these two species (Figure ~~S6~~S5), while correlation for BrC absorption at 440 nm was not significant.

4 Conclusions

In the urban area of Modena, a town representative of ~~large part of~~ several urban areas in the Po valley ~~,~~ (a pollution hotspot for Europe), a set of Light Absorption Aerosol (LAA) observations at multiple wavelengths were collected, along with meteorological and vehicle traffic data. Aerosol absorption was monitored by two *in-situ* MicroAethalometers (MA200), and by a Cimel CE-318 sun/~~sky-photomer~~ sky-photometer contributing to the AERONET network~~: the formers~~ . The MA200 instruments were deployed at two locations representative of urban background and urban traffic conditions in Modena, while the ~~latter~~ Cimel sunphotometer was located in urban background conditions in Modena. In-situ observations, apportioned to fossil fuel and biomass burning, were shown to be largely influenced by ground emissions. The comparison of columnar absorption and *in-situ* absorption rescaled over the mixing-layer exhibited contrasting results, demonstrated by a large difference in the infrared region (mean normalised error, MNE, up to 2.2) but with better agreement in the blue wavelength region (MNE = 0.8), confirming the impact of ground emissions on atmospheric levels of LAA. Under the (reasonable) assumption of the generation of most of the AOD signal within the mixing layer, the heating rate by LAA was estimated in 1.61 $\mathrm{K\,d^{-1}}$. The apportionment of columnar absorption to Black Carbon (BC), Brown Carbon (BrC) and dust, along with the aerosol size distribution by AERONET inversion, highlighted the major role of long-range transported dust in driving the correspondence between the *in-situ* and the columnar absorption at 440 nm, indicating a deeper vertical mixing for dust, ~~contrarily~~ in contrast to urban ground-based emissions which are confined ~~at~~ to lower heights. This latter result was shown specifically for BrC absorption, whose contribution to *in-situ* absorption resulted in a larger contribution to absorption (up to 23%) and featured ~~by~~ wider variability, relative to the columnar retrieval of absorption. The spatial extent of the dust impact was evaluated by the combined analysis of concurrent columnar retrievals in Modena and in Ispra (225 km NW of Modena): the sites showed large agreement in AOD (Pearson's linear correlation coefficient r = 0.84 at 1020 nm) and in AAOD at 440 nm (r = 0.70), where dust has a significant absorption. Consistently the AAOD apportioned to dust was the species with the largest correlation between the two sites, reaching r = 0.62 at 440 nm, supporting the occurrence of ~~also a~~ significant spatial mixing ~~in~~ by the transported dust, along with the vertical mixing.

An improved knowledge of the role by the in-urban emissions of LAA is critical to control local air quality, urban heat island effects and climate forcing and an apportionment of LAA based on their atmospheric levels, as presented here, contributes towards this goal. This study provides important insights on the role of the in-situ absorption monitoring in estimating the actual absorption aloft and whether it can be used for radiative forcing estimates. Moreover the characterization of the intra-urban variation of absorbing aerosol based on different site types contributes in the ambient exposure domain. Towards this latter

Table A1. Statistical metrics for the assessment of the agreement between th in-situ and the columnar data (L^{is} and L_i^{col} respectively)

Mean Error (ME)	$\frac{1}{N}\sum_{i=1}^{N}\left(L_i^{\mathrm{is}} - L_i^{\mathrm{col}}\right)$
Mean Normalised Error (MNE)	$\frac{1}{N}\sum_{i=1}^{N}\frac{\left(L_i^{\mathrm{is}} - L_i^{\mathrm{col}}\right)}{L_i^{\mathrm{col}}}$

outcome, a more in depth investigation of the contribution of urban areas to atmospheric LAA can be gained by the application of specific atmospheric dispersion tools, and this represents one of the major study outlooks. More specifically, Lagrangian particle dispersion models would provide information on atmospheric levels across the urban area at a fine spatial resolution, supporting advanced exposure studies, and, further, would give an estimate of the spatial- and time-resolved emission factors for LAA in the urban area.

Appendix A: AAOD apportionment model

AAOD was apportioned by solving the following equation system

$$\mathrm{AAOD}_\lambda = \sum_i \mathrm{AAOD}_\lambda^i \tag{A1}$$

$$\mathrm{AAOD}_\lambda^i = \mathrm{AAOD}_{\mathrm{ref}}(\lambda/\lambda_{\mathrm{ref}})^{-\mathrm{AAE}_\lambda^i} \tag{A2}$$

with i in BC, Dust and BrC and λ in 440 nm, 675 nm and 880 nm (BrC only at 440 nm and 675 nm).

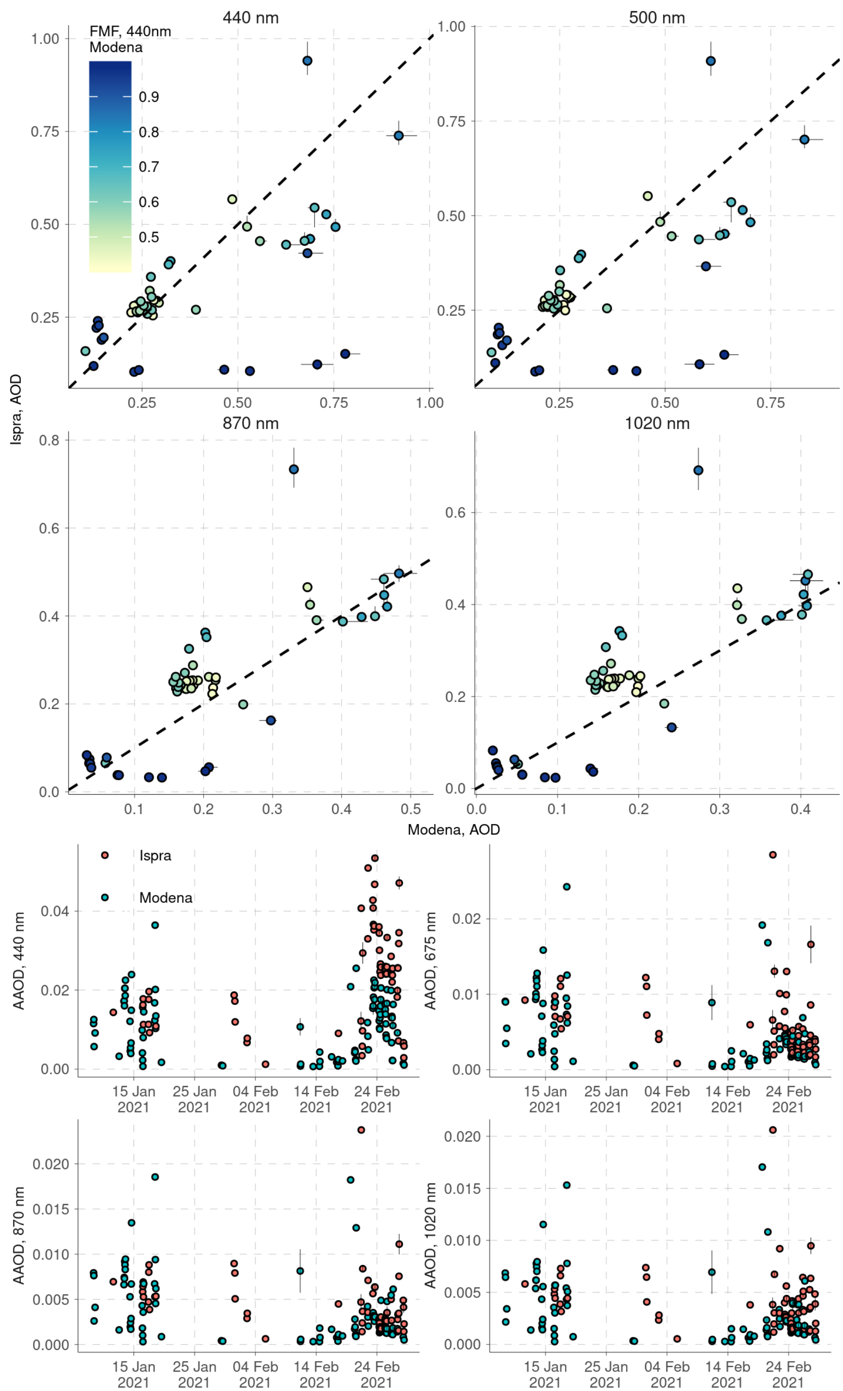

Figure 10. Top panel: comparison of hourly median AOD retrieved in Modena and Ispra at 4 wavelength during the investigated period (January 2020 – March 2021), color-coded according to the Fine Mode Fraction (FMF) at 440 nm. The dashed line indicates the 1:1 line. Lower panel: timeseries in Modena and Ispra of AOD and FMF at 440 nm during the investigated period (January 2020 – March 2021). The bars indicate the hourly interquartile range.

Appendix B: Symbol and acronyms

Table B1. Description of symbols and acronyms used in the text.

Symbol	Description
σ_{ap}	Aerosol particle absorption coefficient
$\sigma_{\mathrm{ap}}^{\mathrm{BC,\,ff}}$	σ_{ap} from BC by fossil fuel combustion
$\sigma_{\mathrm{ap}}^{\mathrm{BC,\,bb}}$	σ_{ap} from BC by biomass burning
$\sigma_{\mathrm{ap}}^{\mathrm{BrC}}$	σ_{ap} by Brown Carbon
$\mathrm{AAE^{c}}$	Absorption Ångström exponent for column observations
$\mathrm{AAE^{c}1}$	$\mathrm{AAE^{c}}$ across the 440 – 675 nm range
$\mathrm{AAE^{c}2}$	$\mathrm{AAE^{c}}$ across the 675 – 880 nm range
$\mathrm{AAE^{i}}$	Absorption Ångström exponent for in-situ observations
$\mathrm{AAE^{i}}_{\mathrm{ff,BC}}$	$\mathrm{AAE^{i}}$ from BC by fossil fuel combustion
$\mathrm{AAE^{i}}_{\mathrm{BrC}}$	$\mathrm{AAE^{i}}$ from BrC
$\mathrm{AAOD}_{\lambda,\,species}$	Absorption AOD at wavelength λ and *species* (i.e. BC, BrC or dust)
ADRE	Absorptive DRE
AERONET	AErosol RObotic NETwork
AOD_{λ}	AOD at wavelength λ
~~ApAOD~~ ApAOH	Apparent ~~AOD~~Aerosol Optical Height
BOA	Bottom of the atmosphere
BC	Black Carbon
BL	Boundary layer
BrC	Brown Carbon
DRE	Direct radiative effect
eBC	equivalent Black Carbon
FMF_{λ}	Fine mode fraction at wavelength λ
HR	Heating rate
IQR	Interquartile range
LAA	Light absorbing aerosol
ME	Mean error
MLH	Mixing layer height
MNE	Mean normalised error
MWAA	Multi-wavelength absorption analyzer
$\mathrm{SAE^{c}}$	Scattering Ångström Exponent for columnar observations
$\mathrm{SAE^{c}1}$	$\mathrm{SAE^{c}}$ across the 440 – 675 nm range
$\mathrm{SAE^{c}2}$	$\mathrm{SAE^{c}}$ across the 675 – 880 nm range
SAOD	Scattering AOD
SSA	column single-scattering albedo
TOA	Top of atmosphere
UB	Urban background
UT	Urban traffic

Code and data availability. ~~In case of publication,~~ We provide:

– the ~~source code for the~~ implementation in R programming language of the ~~AE33~~ dual spot correction ~~on the MA200 raw counts (Drinovec et al., 2015)~~algorithm following Drinovec et al. (2015), which was used for 1-minute urban background data (Bigi, 2023, version 1.0.0 at http://doi.org/xxxx/zenodo.xxxx, last access: xxx). This open-source code is distributed under the ~~source~~ BSD-3 License.

– the R code for the apportionment of the AERONET ~~observations (Bahadur et al., 2012) and raw~~ data according to Bahadur et al. (2012) (Bigi, 2023, version 1.0.0 at http://doi.org/xxxx/zenodo.xxx, last access: xxx). This open-source code is distributed under the BSD-3 License.

– Raw *in-situ* absorption data for Modena ~~will be released~~ (Bigi, 2023, version 1.0.0 at ~~Zenodo~~http://doi.org/xxxx/zenodo.xxx, last access: xxx). The latest version of these tools are available in dedicated GitHub repositories (https://github.com/abigmo/ae33_dualspot_correction and https://github.com/abigmo/aaod_apportionment, last access: XXX).

AERONET data are publicly available at ~~https://aeronet~~the https://aeronet.gsfc.nasa.gov/. ~~gsfc.nasa.gov/.~~ Regulatory air quality ~~and meteorological~~ data for Modena are publicly available both at https://dati.arpae.it/ and on the European Environmental Agency air quality portal. Meteorological data for Modena are publicly available at https://dati.arpae.it/.

Author contributions. AB designed the study, acquired the funds for the absorption in-situ measurements, led the writing of the manuscript and the data analysis. GV, EA, MCC, VB, DM, LF and GG contributed to the development of the methodology and to data interpretation. ST and LG funded and maintained the sun photometer. DM ran the MWAA code. LF computed the HR. All authors contributed to the manuscript.

Competing interests. The authors declare no competing interests.

Acknowledgements. This study was supported by the project ‘Black Air’ (CUP E94I19001080005) funded by the University of Modena and Reggio Emilia and the *Fondazione di Modena* under the programme “Fondo di Ateneo per la Ricerca 2019”. These results were also obtained within the MUSA – Multilayered Urban Sustainability Action – project, funded by the European Union – NextGenerationEU, under the National Recovery and Resilience Plan (NRRP) Mission 4 Component 2 Investment Line 1.5: Strenghtening of research structures and creation of R&D “innovation ecosystems”, set up of “territorial leaders in R&D”. LF acknowledges the GEMMA Center in the framework of the project TECLA, MIUR ’Dipartimenti di Eccellenza 2023-2027’. EA was supported by NOAA cooperative agreements NA17OAR4320101 and NA22OAR4320151. Carla Barbieri and Enrica Canossa from ARPAE are kindly acknowledged for hosting the filter absorption photometers in the air quality monitoring stations and for granting full access to these sites. The municipality of Modena is kindly acknowledged for providing the vehicular traffic data. Hersbach et al. (2018) was downloaded from the Copernicus Climate Change Service (C3S) Climate Data Store: the results contain modified Copernicus Climate Change Service information 2020 and neither the European Commission nor ECMWF is responsible for any use that may be made of the Copernicus information or data it contains. We thank Giuseppe Zibordi and his staff for establishing and maintaining the Ispra AERONET site used in this investigation.

References

Acevedo, O. C., Maroneze, R., Costa, F. D., Puhales, F. S., Degrazia, G. A., Nogueira Martins, L. G., Soares de Oliveira, P. E., and Mortarini, L.: The nocturnal boundary layer transition from weakly to very stable. Part I: Observations, Quarterly Journal of the Royal Meteorological Society, 145, 3577–3592, https://doi.org/10.1002/qj.3642, 2019.

Alas, H. D. C., Müller, T., Weinhold, K., Pfeifer, S., Glojek, K., Gregorič, A., Močnik, G., Drinovec, L., Costabile, F., Ristorini, M., and Wiedensohler, A.: Performance of microAethalometers: Real-world Field Intercomparisons from Multiple Mobile Measurement Campaigns in Different Atmospheric Environments, Aerosol and Air Quality Research, 20, 2640–2653, https://doi.org/10.4209/aaqr.2020.03.0113, 2020.

Andreae, M. O. and Gelencsér, A.: Black carbon or brown carbon? The nature of light-absorbing carbonaceous aerosols, Atmospheric Chemistry and Physics, 6, 3131–3148, https://doi.org/10.5194/acp-6-3131-2006, 2006.

Andrews, E., Ogren, J. A., Kinne, S., and Samset, B.: Comparison of AOD, AAOD and column single scattering albedo from AERONET retrievals and in situ profiling measurements, Atmospheric Chemistry and Physics, 17, 6041–6072, https://doi.org/10.5194/acp-17-6041-2017, 2017.

ARPAE: Update on the Emilia Romagna regional inventory of atmospheric emissions for the year 2017 (in Italian), Tech. rep., ARPAE, 2020.

Aryal, R. P., Voss, K. J., Terman, P. A., Keene, W. C., Moody, J. L., Welton, E. J., and Holben, B. N.: Comparison of surface and column measurements of aerosol scattering properties over the western North Atlantic Ocean at Bermuda, Atmospheric Chemistry and Physics, 14, 7617–7629, https://doi.org/10.5194/acp-14-7617-2014, 2014.

Bahadur, R., Praveen, P. S., Xu, Y., and Ramanathan, V.: Solar absorption by elemental and brown carbon determined from spectral observations, Proceedings of the National Academy of Scicences, 109, 17 366–17 371, https://doi.org/10.1073/pnas.1205910109, 2012.

Barnaba, F., Putaud, J. P., Gruening, C., Dell'Acqua, A., and Dos Santos, S.: Annual cycle in co-located in situ, total-column, and height-resolved aerosol observations in the Po Valley (Italy): Implications for ground-level particulate matter mass concentration estimation from remote sensing, Journal of Geophysical Research: Atmospheres, 115, https://doi.org/10.1029/2009JD013002, 2010.

Battisti, A., Acevedo, O. C., Costa, F. D., Puhales, F. S., Anabor, V., and Degrazia, G. A.: Evaluation of Nocturnal Temperature Forecasts Provided by the Weather Research and Forecast Model for Different Stability Regimes and Terrain Characteristics, Boundary-Layer Meteorology, 162, 523–546, https://doi.org/10.1007/s10546-016-0209-y, 2017.

Bellucci, P. and Cipriani, E.: Data accuracy on automatic traffic counting: the SMART project results, European Transport Research Review, 2, 175–187, https://doi.org/10.1007/s12544-010-0039-9, 2010.

Bergin, M. H., Schwartz, S. E., Halthore, R. N., Ogren, J. A., and Hlavka, D. L.: Comparison of aerosol optical depth inferred from surface measurements with that determined by Sun photometry for cloud-free conditions at a continental U.S. site, Journal of Geophysical Research: Atmospheres, 105, 6807–6816, https://doi.org/10.1029/1999JD900454, 2000.

Bernardoni, V., Vecchi, R., Valli, G., Piazzalunga, A., and Fermo, P.: PM10 source apportionment in Milan (Italy) using time-resolved data, Science of The Total Environment, 409, 4788–4795, https://doi.org/10.1016/j.scitotenv.2011.07.048, 2011.

Bernardoni, V., Calzolai, G., Chiari, M., Fedi, M., Lucarelli, F., Nava, S., Piazzalunga, A., Riccobono, F., Taccetti, F., Valli, G., and Vecchi, R.: Radiocarbon analysis on organic and elemental carbon in aerosol samples and source apportionment at an urban site in Northern Italy, Journal of Aerosol Science, 56, 88–99, https://doi.org/10.1016/j.jaerosci.2012.06.001, special Issue: 10th International Conference on Carbonaceous Particles in the Atmosphere, Vienna, Austria, 2011, 2013.

Bernardoni, V., Pileci, R. E., Caponi, L., and Massabò, D.: The Multi-Wavelength Absorption Analyzer (MWAA) Model as a Tool for Source and Component Apportionment Based on Aerosol Absorption Properties: Application to Samples Collected in Different Environments, Atmosphere, 8, https://doi.org/10.3390/atmos8110218, 2017.

Bigi, A. and Ghermandi, G.: Long-term trend and variability of atmospheric PM_{10} concentration in the Po Valley, Atmospheric Chemistry and Physics, 14, 4895–4907, https://doi.org/10.5194/acp-14-4895-2014, 2014.

Bigi, A. and Ghermandi, G.: Trends and variability of atmospheric $PM_{2.5}$ and $PM_{10-2.5}$ concentration in the Po Valley, Italy, Atmospheric Chemistry and Physics, 16, 15 777–15 788, https://doi.org/10.5194/acp-16-15777-2016, 2016.

Bond, T. C., Doherty, S. J., Fahey, D. W., Forster, P. M., Berntsen, T., DeAngelo, B. J., Flanner, M. G., Ghan, S., Kärcher, B., Koch, D., Kinne, S., Kondo, Y., Quinn, P. K., Sarofim, M. C., Schultz, M. G., Schulz, M., Venkataraman, C., Zhang, H., Zhang, S., Bellouin, N., Guttikunda, S. K., Hopke, P. K., Jacobson, M. Z., Kaiser, J. W., Klimont, Z., Lohmann, U., Schwarz, J. P., Shindell, D., Storelvmo, T., Warren, S. G., and Zender, C. S.: Bounding the role of black carbon in the climate system: a scientific assessment, Journal of Geophysical Research: Atmospheres, 118, 5380–5552, https://doi.org/10.1002/jgrd.50171, 2013.

Boniardi, L., Dons, E., Longhi, F., Scuffi, C., Campo, L., Van Poppel, M., Int Panis, L., and Fustinoni, S.: Personal exposure to equivalent black carbon in children in Milan, Italy: Time-activity patterns and predictors by season, Environmental Pollution, 274, 116 530, https://doi.org/10.1016/j.envpol.2021.116530, 2021.

Brown, H., Liu, X., Feng, Y., Jiang, Y., Wu, M., Lu, Z., Wu, C., Murphy, S., and Pokhrel, R.: Radiative effect and climate impacts of brown carbon with the Community Atmosphere Model (CAM5), Atmospheric Chemistry and Physics, 18, 17 745–17 768, https://doi.org/10.5194/acp-18-17745-2018, 2018.

Carslaw, D. C. and Ropkins, K.: openair — An R package for air quality data analysis, Environmental Modelling & Software, 27–28, 52–61, https://doi.org/10.1016/j.envsoft.2011.09.008, 2012.

Cazorla, A., Bahadur, R., Suski, K. J., Cahill, J. F., Chand, D., Schmid, B., Ramanathan, V., and Prather, K. A.: Relating aerosol absorption due to soot, organic carbon, and dust to emission sources determined from in-situ chemical measurements, Atmospheric Chemistry and Physics, 13, 9337–9350, https://doi.org/10.5194/acp-13-9337-2013, 2013.

Chakrabarty, R. K., Garro, M. A., Wilcox, E. M., and Moosmüller, H.: Strong radiative heating due to wintertime black carbon aerosols in the Brahmaputra River Valley, Geophysical Research Letters, 39, https://doi.org/10.1029/2012GL051148, 2012.

Charlson, R. J., Schwartz, S. E., Hales, J. M., Cess, R. D., Coakley, J. A., Hansen, J. E., and Hofmann, D. J.: Climate forcing by anthropogenic aerosols, Science, 255, 423–430, https://doi.org/10.1126/science.255.5043.423, 1992.

Chauvigné, A., Sellegri, K., Hervo, M., Montoux, N., Freville, P., and Goloub, P.: Comparison of the aerosol optical properties and distribution retrieved by sun photometer with in situ measurements at midlatitude, Atmospheric Measurement Techniques, 9, 4569–4585, https://doi.org/10.5194/amt-9-4569-2016, 2016.

Chen, S., Russell, L. M., Cappa, C. D., Zhang, X., Kleeman, M. J., Kumar, A., Liu, D., and Ramanathan, V.: Comparing black and brown carbon absorption from AERONET and surface measurements at wintertime Fresno, Atmospheric Environment, 199, 164–176, https://doi.org/10.1016/j.atmosenv.2018.11.032, 2019.

Cho, C., Kim, S.-W., Lee, M., Lim, S., Fang, W., Gustafsson, O., Andersson, A., Park, R. J., and Sheridan, P. J.: Observation-based estimates of the mass absorption cross-section of black and brown carbon and their contribution to aerosol light absorption in East Asia, Atmospheric Environment, 212, 65–74, https://doi.org/10.1016/j.atmosenv.2019.05.024, 2019.

Chowdhury, P. H., He, Q., Carmieli, R., Li, C., Rudich, Y., and Pardo, M.: Connecting the Oxidative Potential of Secondary Organic Aerosols with Reactive Oxygen Species in Exposed Lung Cells, Environ. Sci. Technol., 53, 13 949–13 958, https://doi.org/10.1021/acs.est.9b04449, 2019.

Chung, C. E., Ramanathan, V., and Decremer, D.: Observationally constrained estimates of carbonaceous aerosol radiative forcing, Proceedings of the National Academy of Sciences, 109, 11 624–11 629, https://doi.org/10.1073/pnas.1203707109, 2012.

Ciarelli, G., Jiang, J., El Haddad, I., Bigi, A., Aksoyoglu, S., Prévôt, A. S. H., Marinoni, A., Shen, J., Yan, C., and Bianchi, F.: Modeling the effect of reduced traffic due to COVID-19 measures on air quality using a chemical transport model: impacts on the Po Valley and the Swiss Plateau regions, Environmental Science: Atmospheres, 1, 228–240, https://doi.org/10.1039/D1EA00036E, 2021.

Clerici, M. and Mélin, F.: Aerosol direct radiative effect in the Po Valley region derived from AERONET measurements, Atmospheric Chemistry and Physics, 8, 4925–4946, https://doi.org/10.5194/acp-8-4925-2008, 2008.

Cleveland, W. S., Graedel, T. E., Kleiner, B., and Warner, J. L.: Sunday and Workday Variations in Photochemical Air Pollutants in New Jersey and New York, Science, 186, 1037–1038, https://doi.org/10.1126/science.186.4168.1037, 1974.

Cohen, A. J., Brauer, M., Burnett, R., Anderson, H. R., Frostad, J., Estep, K., Balakrishnan, K., Brunekreef, B., Dandona, L., Dandona, R., Feigin, V., Freedman, G., Hubbell, B., Jobling, A., Kan, H., Knibbs, L., Liu, Y., Martin, R., Morawska, L., Pope, C. A., Shin, H., Straif, K., Shaddick, G., Thomas, M., van Dingenen, R., van Donkelaar, A., Vos, T., Murray, C. J. L., and Forouzanfar, M. H.: Estimates and 25-year trends of the global burden of disease attributable to ambient air pollution: an analysis of data from the Global Burden of Diseases Study 2015, The Lancet, 389, 1907–1918, https://doi.org/10.1016/S0140-6736(17)30505-6, 2017.

Collaud Coen, M., Weingartner, E., Apituley, A., Ceburnis, D., Fierz-Schmidhauser, R., Flentje, H., Henzing, J. S., Jennings, S. G., Moerman, M., Petzold, A., Schmid, O., and Baltensperger, U.: Minimizing light absorption measurement artifacts of the Aethalometer: evaluation of five correction algorithms, Atmospheric Measurement Techniques, 3, 457–474, https://doi.org/10.5194/amt-3-457-2010, 2010.

Collaud Coen, M., Andrews, E., Alastuey, A., Arsov, T. P., Backman, J., Brem, B. T., Bukowiecki, N., Couret, C., Eleftheriadis, K., Flentje, H., Fiebig, M., Gysel-Beer, M., Hand, J. L., Hoffer, A., Hooda, R., Hueglin, C., Joubert, W., Keywood, M., Kim, J. E., Kim, S.-W., Labuschagne, C., Lin, N.-H., Lin, Y., Lund Myhre, C., Luoma, K., Lyamani, H., Marinoni, A., Mayol-Bracero, O. L., Mihalopoulos, N., Pandolfi, M., Prats, N., Prenni, A. J., Putaud, J.-P., Ries, L., Reisen, F., Sellegri, K., Sharma, S., Sheridan, P., Sherman, J. P., Sun, J., Titos, G., Torres, E., Tuch, T., Weller, R., Wiedensohler, A., Zieger, P., and Laj, P.: Multidecadal trend analysis of in situ aerosol radiative properties around the world, Atmospheric Chemistry and Physics, 20, 8867–8908, https://doi.org/10.5194/acp-20-8867-2020, 2020.

Costabile, F., Gilardoni, S., Barnaba, F., Di Ianni, A., Di Liberto, L., Dionisi, D., Manigrasso, M., Paglione, M., Poluzzi, V., Rinaldi, M., Facchini, M. C., and Gobbi, G. P.: Characteristics of brown carbon in the urban Po Valley atmosphere, Atmospheric Chemistry and Physics, 17, 313–326, https://doi.org/10.5194/acp-17-313-2017, 2017.

Das, S. K. and Jayaraman, A.: Role of black carbon in aerosol properties and radiative forcing over western India during premonsoon period, Atmospheric Research, 102, 320–334, https://doi.org/10.1016/j.atmosres.2011.08.003, 2011.

Drinovec, L., Močnik, G., Zotter, P., Prévôt, A. S. H., Ruckstuhl, C., Coz, E., Rupakheti, M., Sciare, J., Müller, T., Wiedensohler, A., and Hansen, A. D. A.: The dual-spot Aethalometer: an improved measurement of aerosol black carbon with real-time loading compensation, Atmospheric Measurement Techniques, 8, 1965–1979, https://doi.org/10.5194/amt-8-1965-2015, 2015.

Drinovec, L., Jagodič, U., Pirker, L., Škarabot, M., Kurtjak, M., Vidović, K., Ferrero, L., Visser, B., Röhrbein, J., Weingartner, E., Kalbermatter, D. M., Vasilatou, K., Bühlmann, T., Pascale, C., Müller, T., Wiedensohler, A., and Močnik, G.: A dual-wavelength photothermal aerosol absorption monitor: design, calibration and performance, Atmospheric Measurement Techniques, 15, 3805–3825, https://doi.org/10.5194/amt-15-3805-2022, 2022.

Dubovik, O., Smirnov, A., Holben, B. N., King, M. D., Kaufman, Y. J., Eck, T. F., and Slutsker, I.: Accuracy assessments of aerosol optical properties retrieved from Aerosol Robotic Network (AERONET) Sun and sky radiance measurements, Journal of Geophysical Research: Atmospheres, 105, 9791–9806, https://doi.org/10.1029/2000JD900040, 2000.

Dubovik, O., Holben, B., Eck, T. F., Smirnov, A., Kaufman, Y. J., King, M. D., Tanré, D., and Slutsker, I.: Variability of Absorption and Optical Properties of Key Aerosol Types Observed in Worldwide Locations, Journal of the Atmospheric Sciences, 59, 590–608, https://doi.org/10.1175/1520-0469(2002)059<0590:VOAAOP>2.0.CO;2, 2002.

Dubovik, O., Lapyonok, T., Litvinov, P., Herman, M., Fuertes, M., Ducos, F., Torres, B., Derimian, Y., Huang, X., Lopatin, A., Chaikovsky, A., Aspetsberger, M., and Federspiel, C.: GRASP: a versatile algorithm for characterizing the atmosphere, SPIE: Newsroom, https://doi.org/10.1117/2.1201408.005558, published Online: September 19, 2014, 2014.

Ealo, M., Alastuey, A., Pérez, N., Ripoll, A., Querol, X., and Pandolfi, M.: Impact of aerosol particle sources on optical properties in urban, regional and remote areas in the north-western Mediterranean, Atmospheric Chemistry and Physics, 18, 1149–1169, https://doi.org/10.5194/acp-18-1149-2018, 2018.

Eck, T. F., Holben, B. N., Reid, J. S., Dubovik, O., Smirnov, A., O'Neill, N. T., Slutsker, I., and Kinne, S.: Wavelength dependence of the optical depth of biomass burning, urban, and desert dust aerosols, Journal of Geophysical Research: Atmospheres, 104, 31 333–31 349, https://doi.org/10.1029/1999JD900923, 1999.

ECMWF: IFS DOCUMENTATION – Cy43r3 Operational implementation 11 July 2017 PART IV: PHYSICAL PROCESSES, 2017.

European Environment Agency: Status of black carbon monitoring in ambient air in Europe, Tech. Rep. 18/2013, Publications Office, Luxembourg, https://data.europa.eu/doi/10.2800/10150, 2013.

Evangeliou, N., Platt, S. M., Eckhardt, S., Lund Myhre, C., Laj, P., Alados-Arboledas, L., Backman, J., Brem, B. T., Fiebig, M., Flentje, H., Marinoni, A., Pandolfi, M., Yus-Dìez, J., Prats, N., Putaud, J. P., Sellegri, K., Sorribas, M., Eleftheriadis, K., Vratolis, S., Wiedensohler, A., and Stohl, A.: Changes in black carbon emissions over Europe due to COVID-19 lockdowns, Atmospheric Chemistry and Physics, 21, 2675–2692, https://doi.org/10.5194/acp-21-2675-2021, 2021.

Feng, Y., Ramanathan, V., and Kotamarthi, V. R.: Brown carbon: a significant atmospheric absorber of solar radiation?, Atmospheric Chemistry and Physics, 13, 8607–8621, https://doi.org/10.5194/acp-13-8607-2013, 2013.

Ferrero, L., Močnik, G., Ferrini, B., Perrone, M., Sangiorgi, G., and Bolzacchini, E.: Vertical profiles of aerosol absorption coefficient from micro-Aethalometer data and Mie calculation over Milan, Science of The Total Environment, 409, 2824–2837, https://doi.org/10.1016/j.scitotenv.2011.04.022, 2011.

Ferrero, L., Castelli, M., Ferrini, B. S., Moscatelli, M., Perrone, M. G., Sangiorgi, G., D'Angelo, L., Rovelli, G., Moroni, B., Scardazza, F., Močnik, G., Bolzacchini, E., Petitta, M., and Cappelletti, D.: Impact of black carbon aerosol over Italian basin valleys: high-resolution measurements along vertical profiles, radiative forcing and heating rate, Atmospheric Chemistry and Physics, 14, 9641–9664, https://doi.org/10.5194/acp-14-9641-2014, 2014.

Ferrero, L., Močnik, G., Cogliati, S., Gregorič, A., Colombo, R., and Bolzacchini, E.: Heating Rate of Light Absorbing Aerosols: Time-Resolved Measurements, the Role of Clouds, and Source Identification, Environmental Science & Technology, 52, 3546–3555, https://doi.org/10.1021/acs.est.7b04320, 2018.

Ferrero, L., Riccio, A., Ferrini, B. S., D'Angelo, L., Rovelli, G., Casati, M., Angelini, F., Barnaba, F., Gobbi, G. P., Cataldi, M., and Bolzacchini, E.: Satellite AOD conversion into ground PM_{10}. $PM_{2.5}$ and PM_1 over the Po valley (Milan, Italy) exploiting information on aerosol vertical profiles, chemistry, hygroscopicity and meteorology, Atmospheric Pollution Research, 10, 1895–1912, https://doi.org/10.1016/j.apr.2019.08.003, 2019.

Ferrero, L., Bernardoni, V., Santagostini, L., Cogliati, S., Soldan, F., Valentini, S., D., M., Močnik, G., Gregorič, A., Rigler, M., Prati, P., Bigogno, A., Losi, N., Valli, G., Vecchi, R., and Bolzacchini, E.: Consistent determination of the heating rate of light-absorbing aerosol using wavelength- and time-dependent Aethalometer multiple-scattering correction, Science of The Total Environment, 791, 148 277, https://doi.org/10.1016/j.scitotenv.2021.148277, 2021a.

Ferrero, L., Gregorič, A., Močnik, G., Rigler, M., Cogliati, S., Barnaba, F., Di Liberto, L., Gobbi, G. P., Losi, N., and Bolzacchini, E.: The impact of cloudiness and cloud type on the atmospheric heating rate of black and brown carbon in the Po Valley, Atmospheric Chemistry and Physics, 21, 4869–4897, https://doi.org/10.5194/acp-21-4869-2021, 2021b.

Forster, P., Storelvmo, T., Armour, K., Collins, W., Dufresne, J.-L., Frame, D., Lunt, D. J., Mauritsen, T., Palmer, M. D., Watanabe, M., Wild, M., and Zhang, H.: Climate Change 2021: The Physical Science Basis. Contribution of Working Group I to the Sixth Assessment Report of the Intergovernmental Panel on Climate Change, vol. 6, chap. The Earth's energy budget, climate feedbacks, and climate sensitivity, p. 204, Cambridge University Press, 2021.

Ghermandi, G., Fabbi, S., Veratti, G., Bigi, A., and Teggi, S.: Estimate of secondary NO_2 levels at two urban traffic sites using observations and modelling, Sustainability (Switzerland), 12, https://doi.org/10.3390/SU12197897, 2020.

Gilardoni, S., Massoli, P., Paglione, M., Giulianelli, L., Carbone, C., Rinaldi, M., Decesari, S., Sandrini, S., Costabile, F., Gobbi, G. P., Pietrogrande, M. C., Visentin, M., Scotto, F., Fuzzi, S., and Facchini, M. C.: Direct observation of aqueous secondary organic aerosol from biomass-burning emissions, Proceedings of the National Academy of Scicences, 113, 10 013–10 018, https://doi.org/10.1073/pnas.1602212113, 2016.

Gilardoni, S., Massoli, P., Marinoni, A., Mazzoleni, C., Freedman, A., Lonati, G., De Iuliis, S., and Gianelle, V.: Spatial and temporal variability of carbonaceous aerosol absorption in the Po Valley, Aerosol and Air Quality Research, 20, 2624–2639, https://doi.org/10.4209/aaqr.2020.03.0085, 2020a.

Gilardoni, S., Tarozzi, L., Sandrini, S., Ielpo, P., Contini, D., Putaud, J.-P., Cavalli, F., Poluzzi, V., Bacco, D., Leonardi, C., Genga, A., Langone, L., and Fuzzi, S.: Reconstructing Elemental Carbon Long-Term Trend in the Po Valley (Italy) from Fog Water Samples, Atmosphere, 11, https://doi.org/10.3390/atmos11060580, 2020b.

Giles, D. M., Holben, B. N., Eck, T. F., Sinyuk, A., Smirnov, A., Slutsker, I., Dickerson, R. R., Thompson, A. M., and Schafer, J. S.: An analysis of AERONET aerosol absorption properties and classifications representative of aerosol source regions, Journal of Geophysical Research: Atmospheres, 117, https://doi.org/10.1029/2012JD018127, 2012.

Good, N., Mölter, A., Peel, J. L., and Volckens, J.: An accurate filter loading correction is essential for assessing personal exposure to black carbon using an Aethalometer, Journal of Exposure Science & Environmental Epidemiology, 27, 409–416, https://doi.org/10.1038/jes.2016.71, 2017.

Grivas, G., Stavroulas, I., Liakakou, E., Kaskaoutis, D. G., Bougiatioti, A., Paraskevopoulou, D., Gerasopoulos, E., and Mihalopoulos, N.: Measuring the spatial variability of black carbon in Athens during wintertime, Air Quality, Atmosphere & Health, 12, 1405–1417, https://doi.org/10.1007/s11869-019-00756-y, 2019.

Guo, J., Zhang, J., Yang, K., Liao, H., Zhang, S., Huang, K., Lv, Y., Shao, J., Yu, T., Tong, B., Li, J., Su, T., Yim, S. H. L., Stoffelen, A., Zhai, P., and Xu, X.: Investigation of near-global daytime boundary layer height using high-resolution radiosondes: first results and comparison with ERA5, MERRA-2, JRA-55, and NCEP-2 reanalyses, Atmospheric Chemistry and Physics, 21, 17 079–17 097, https://doi.org/10.5194/acp-21-17079-2021, 2021.

Heald, C. L., Ridley, D. A., Kroll, J. H., Barrett, S. R. H., Cady-Pereira, K. E., Alvarado, M. J., and Holmes, C. D.: Contrasting the direct radiative effect and direct radiative forcing of aerosols, Atmospheric Chemistry and Physics, 14, 5513–5527, https://doi.org/10.5194/acp-14-5513-2014, 2014.

Hersbach, H., Bell, B., Berrisford, P., Biavati, G., Horányi, A., Muñoz Sabater, J., Nicolas, J., Peubey, C., Radu, R., Rozum, I., Schepers, D., Simmons, A., Soci, C., Dee, D., and Thépaut, J.-N.: ERA5 hourly data on single levels from 1979 to present, https://doi.org/10.24381/cds.adbb2d47, 2018.

Holben, B., Eck, T., Slutsker, I., Tanré, D., Buis, J., Setzer, A., Vermote, E., Reagan, J., Kaufman, Y., Nakajima, T., Lavenu, F., Jankowiak, I., and Smirnover, A.: AERONET – A Federated Instrument Network and Data Archive for Aerosol Characterization, Remote Sensing of Environment, 66, 1–16, https://doi.org/10.1016/S0034-4257(98)00031-5, 1998.

Hyvärinen, A.-P., Vakkari, V., Laakso, L., Hooda, R. K., Sharma, V. P., Panwar, T. S., Beukes, J. P., van Zyl, P. G., Josipovic, M., Garland, R. M., Andreae, M. O., Pöschl, U., and Petzold, A.: Correction for a measurement artifact of the Multi-Angle Absorption Photometer (MAAP) at high black carbon mass concentration levels, Atmospheric Measurement Techniques, 6, 81–90, https://doi.org/10.5194/amt-6-81-2013, 2013.

Janssen, N. A., Gerlofs-Nijland, M. E., Lanki, T., Salonen, R. O., Cassee, F., Hoek, G., Fischer, P., Brunekreef, B., and Krzyzanowsk, M.: Health Effects of Black Carbon, Tech. rep., WHO regional office for Europe, Copenhagen, 2012.

Jo, D. S., Park, R. J., Lee, S., Kim, S.-W., and Zhang, X.: A global simulation of brown carbon: implications for photochemistry and direct radiative effect, Atmospheric Chemistry and Physics, 16, 3413–3432, https://doi.org/10.5194/acp-16-3413-2016, 2016.

Kalbermatter, D. M., Močnik, G., Drinovec, L., Visser, B., Röhrbein, J., Oscity, M., Weingartner, E., Hyvärinen, A.-P., and Vasilatou, K.: Comparing black-carbon- and aerosol-absorption-measuring instruments – a new system using lab-generated soot coated with controlled amounts of secondary organic matter, Atmospheric Measurement Techniques, 15, 561–572, https://doi.org/10.5194/amt-15-561-2022, 2022.

Kaskaoutis, D. G., Grivas, G., Stavroulas, I., Bougiatioti, A., Liakakou, E., Dumka, U. C., Gerasopoulos, E., and Mihalopoulos, N.: Apportionment of black and brown carbon spectral absorption sources in the urban environment of Athens, Greece, during winter, Science of The Total Environment, 801, 149 739, https://doi.org/10.1016/j.scitotenv.2021.149739, 2021.

Katsanos, D., Bougiatioti, A., Liakakou, E., Kaskaoutis, D. G., Stavroulas, I., Paraskevopoulou, D., Lianou, M., Psiloglou, B. E., Gerasopoulos, E., Pilinis, C., and Mihalopoulos, N.: Optical Properties of Near-Surface Urban Aerosols and their Chemical Tracing in a Mediterranean City (Athens), Aerosol and Air Quality Research, 19, 49–70, https://doi.org/10.4209/aaqr.2017.11.0544, 2019.

Kayetha, V., Torres, O., and Jethva, H.: Retrieval of UV–visible aerosol absorption using AERONET and OMI–MODIS synergy: spatial and temporal variability across major aerosol environments, Atmospheric Measurement Techniques, 15, 845–877, https://doi.org/10.5194/amt-15-845-2022, 2022.

Kedia, S., Ramachandran, S., Kumar, A., and Sarin, M. M.: Spatiotemporal gradients in aerosol radiative forcing and heating rate over Bay of Bengal and Arabian Sea derived on the basis of optical, physical, and chemical properties, Journal of Geophysical Research: Atmospheres, 115, https://doi.org/10.1029/2009JD013136, 2010.

Kezoudi, M., Keleshis, C., Antoniou, P., Biskos, G., Bronz, M., Constantinides, C., Desservettaz, M., Gao, R.-S., Girdwood, J., Harnetiaux, J., Kandler, K., Leonidou, A., Liu, Y., Lelieveld, J., Marenco, F., Mihalopoulos, N., Močnik, G., Neitola, K., Paris, J.-D., Pikridas, M., Sarda-Esteve, R., Stopford, C., Unga, F., Vrekoussis, M., and Sciare, J.: The Unmanned Systems Research Laboratory (USRL): A New Facility for UAV-Based Atmospheric Observations, Atmosphere, 12, https://doi.org/10.3390/atmos12081042, 2021.

Kim, S.-W., Cho, C., and Rupakheti, M.: Estimating contributions of black and brown carbon to solar absorption from aethalometer and AERONET measurements in the highly polluted Kathmandu Valley, Nepal, Atmospheric Research, 247, 105 164, https://doi.org/10.1016/j.atmosres.2020.105164, 2021.

Kirrane, E. F., Luben, T. J., Benson, A., Owens, E. O., Sacks, J. D., Dutton, S. J., Madden, M., and Nichols, J. L.: A systematic review of cardiovascular responses associated with ambient black carbon and fine particulate matter, Environment International, 127, 305–316, https://doi.org/10.1016/j.envint.2019.02.027, 2019.

Lack, D. A., Moosmüller, H., McMeeking, G. R., Chakrabarty, R. K., and Baumgardner, D.: Characterizing elemental, equivalent black, and refractory black carbon aerosol particles: a review of techniques, their limitations and uncertainties, Analytical and Bioanalytical Chemistry, 406, 99–122, https://doi.org/10.1007/s00216-013-7402-3, 2014.

Laj, P., Bigi, A., Rose, C., Andrews, E., Lund Myhre, C., Collaud Coen, M., Lin, Y., Wiedensohler, A., Schulz, M., A. Ogren, J., Fiebig, M., Gliß, J., Mortier, A., Pandolfi, M., Petäjä, T., Kim, S.-W., Aas, W., Putaud, J.-P., Mayol-Bracero, O., Keywood, M., Labrador, L., Aalto, P., Ahlberg, E., Alados Arboledas, L., Alastuey, A., Andrade, M., Artinano, B., Ausmeel, S., Arsov, T., Asmi, E., Backman, J., Baltensperger, U., Bastian, S., Bath, O., Paul Beukes, J., T. Brem, B., Bukowiecki, N., Conil, S., Couret, C., Day, D., Dayantolis, W., Degorska, A., Eleftheriadis, K., Fetfatzis, P., Favez, O., Flentje, H., I. Gini, M., Gregorič, A., Gysel-Beer, M., Gannet Hallar, A., Hand, J., Hoffer, A., Hueglin, C., K. Hooda, R., Hyvärinen, A., Kalapov, I., Kalivitis, N., Kasper-Giebl, A., Eun Kim, J., Kouvarakis, G., Kranjc, I., Krejci, R., Kulmala, M., Labuschagne, C., Lee, H.-J., Lihavainen, H., Lin, N.-H., Löschau, G., Luoma, K., Marinoni, A., Martins Dos Santos, S., Meinhardt, F., Merkel, M., Metzger, J.-M., Mihalopoulos, N., Anh Nguyen, N., Ondracek, J., Pérez, N., Perrone, M., Pichon, J.-M., Picard, D., Pichon, J.-M., Pont, V., Prats, N., Prenni, A., Reisen, F., Romano, S., Sellegri, K., Sharma, S., Schauer, G., Sheridan, P., Sherman, J., Schütze, M., Schwerin, A., Sohmer, R., Sorribas, M., Steinbacher, M., Sun, J., Titos, G., Toczko, B., Tuch, T., Tulet, P., Tunved, P., Vakkari, V., Velarde, F., Velasquez, P., Villani, P., Vratolis, S., Wang, S.-H., Weinhold, K., Weller, R., Yela, M., Yus-Diez, J., Zdimal, V., Zieger, P., and Zikova, N.: A global analysis of climate-relevant aerosol properties retrieved from the network of Global Atmosphere Watch (GAW) near-surface observatories, Atmospheric Measurement Techniques, 13, 4353–4392, https://doi.org/10.5194/amt-13-4353-2020, 2020.

Langridge, J. M., Richardson, M. S., Lack, D. A., Brock, C. A., and Murphy, D. M.: Limitations of the Photoacoustic Technique for Aerosol Absorption Measurement at High Relative Humidity, Aerosol Science and Technology, 47, 1163–1173, https://doi.org/10.1080/02786826.2013.827324, 2013.

Lapo, K., Nijssen, B., and Lundquist, J. D.: Evaluation of Turbulence Stability Schemes of Land Models for Stable Conditions, Journal of Geophysical Research: Atmospheres, 124, 3072–3089, https://doi.org/10.1029/2018JD028970, 2019.

Laskin, A., Laskin, J., and Nizkorodov, S. A.: Chemistry of Atmospheric Brown Carbon, Chemical Reviews, 115, 4335–4382, https://doi.org/10.1021/cr5006167, 2015.

Li, C., Windwer, E., Fang, Z., Nissenbaum, D., and Rudich, Y.: Correcting micro-aethalometer absorption measurements for brown carbon aerosol, Science of The Total Environment, 777, 146 143, https://doi.org/10.1016/j.scitotenv.2021.146143, 2021.

Li, C., Misovich, M. V., Pardo, M., Fang, Z., Laskin, A., Chen, J., and Rudich, Y.: Secondary organic aerosol formation from atmospheric reactions of anisole and associated health effects, Chemosphere, 308, 136 421, https://doi.org/https://doi.org/10.1016/j.chemosphere.2022.136421, 2022.

Li, H., McMeeking, G. R., and May, A. A.: Development of a new correction algorithm applicable to any filter-based absorption photometer, Atmospheric Measurement Techniques, 13, 2865–2886, https://doi.org/10.5194/amt-13-2865-2020, 2020.

Li, J., Carlson, B. E., Dubovik, O., and Lacis, A. A.: Recent trends in aerosol optical properties derived from AERONET measurements, Atmospheric Chemistry and Physics, 14, 12 271–12 289, https://doi.org/10.5194/acp-14-12271-2014, 2014.

Liakakou, E., Kaskaoutis, D. G., Grivas, G., Stavroulas, I., Tsagkaraki, M., Paraskevopoulou, D., Bougiatioti, A., Dumka, U. C., Gerasopoulos, E., and Mihalopoulos, N.: Long-term brown carbon spectral characteristics in a Mediterranean city (Athens), Science of The Total Environment, 708, 135 019, https://doi.org/10.1016/j.scitotenv.2019.135019, 2020.

Lin, G., Penner, J. E., Flanner, M. G., Sillman, S., Xu, L., and Zhou, C.: Radiative forcing of organic aerosol in the atmosphere and on snow: Effects of SOA and brown carbon, Journal of Geophysical Research: Atmospheres, 119, 7453–7476, https://doi.org/10.1002/2013JD021186, 2014.

Liu, C., Chung, C. E., Yin, Y., and Schnaiter, M.: The absorption Ångström exponent of black carbon: from numerical aspects, Atmospheric Chemistry and Physics, 18, 6259–6273, https://doi.org/10.5194/acp-18-6259-2018, 2018.

Liu, M., Peng, X., Meng, Z., Zhou, T., Long, L., and She, Q.: Spatial characteristics and determinants of in-traffic black carbon in Shanghai, China: Combination of mobile monitoring and land use regression model, Science of The Total Environment, 658, 51–61, https://doi.org/10.1016/j.scitotenv.2018.12.135, 2019.

Liu, X., Hadiatullah, H., Zhang, X., Hill, L. D., White, A. H. A., Schnelle-Kreis, J., Bendl, J., Jakobi, G., Schloter-Hai, B., and Zimmermann, R.: Analysis of mobile monitoring data from the microAeth® MA200 for measuring changes in black carbon on the roadside in Augsburg, Atmospheric Measurement Techniques, 14, 5139–5151, https://doi.org/10.5194/amt-14-5139-2021, 2021.

Loía-Salazar, S. M., Arnott, W. P., and Moosmüller, H.: Accuracy of near-surface aerosol extinction determined from columnar aerosol optical depth measurements in Reno, NV, USA, Journal of Geophysical Research: Atmospheres, 119, 11,355–11,374, https://doi.org/10.1002/2014JD022138, 2014.

Loomis, D., Grosse, Y., Lauby-Secretan, B., Ghissassi, F. E., Bouvard, V., Benbrahim-Tallaa, L., Guha, N., Baan, R., Mattock, H., and Straif, K.: The carcinogenicity of outdoor air pollution, The Lancet Oncology, 14, 1262–1263, https://doi.org/10.1016/S1470-2045(13)70487-X, 2013.

Luben, T. J., Nichols, J. L., Dutton, S. J., Kirrane, E., Owens, E. O., Datko-Williams, L., Madden, M., and Sacks, J. D.: A systematic review of cardiovascular emergency department visits, hospital admissions and mortality associated with ambient black carbon, Environment International, 107, 154–162, https://doi.org/10.1016/j.envint.2017.07.005, 2017.

Magalhaes, S., Baumgartner, J., and Weichenthal, S.: Impacts of exposure to black carbon, elemental carbon, and ultrafine particles from indoor and outdoor sources on blood pressure in adults: A review of epidemiological evidence, Environmental Research, 161, 345–353, https://doi.org/10.1016/j.envres.2017.11.030, 2018.

Mahrt, L.: Stably Stratified Atmospheric Boundary Layers, Annual Review of Fluid Mechanics, 46, 23–45, https://doi.org/10.1146/annurev-fluid-010313-141354, 2014.

Mallet, M., Dubovik, O., Nabat, P., Dulac, F., Kahn, R., Sciare, J., Paronis, D., and Léon, J. F.: Absorption properties of Mediterranean aerosols obtained from multi-year ground-based remote sensing observations, Atmospheric Chemistry and Physics, 13, 9195–9210, https://doi.org/10.5194/acp-13-9195-2013, 2013.

Maroneze, R., Acevedo, O. C., Costa, F. D., Puhales, F. S., Anabor, V., Lemes, D. N., and Mortarini, L.: How is the Two-Regime Stable Boundary Layer Reproduced by the Different Turbulence Parametrizations in the Weather Research and Forecasting Model?, Boundary-Layer Meteorology, 178, 383–413, https://doi.org/10.1007/s10546-020-00581-2, 2021.

Martilli, A., Sanchez, B., Rasilla, D., Pappaccogli, G., Allende, F., Martin, F., Román-Cascón, C., Yagüe, C., and Fernandez, F.: Simulating the meteorology during persistent Wintertime Thermal Inversions over urban areas. The case of Madrid, Atmospheric Research, 263, 105 789, https://doi.org/10.1016/j.atmosres.2021.105789, 2021.

Massabò, D., Caponi, L., Bernardoni, V., Bove, M., Brotto, P., Calzolai, G., Cassola, F., Chiari, M., Fedi, M., Fermo, P., Giannoni, M., Lucarelli, F., Nava, S., Piazzalunga, A., Valli, G., Vecchi, R., and Prati, P.: Multi-wavelength optical determination of black and brown carbon in atmospheric aerosols, Atmospheric Environment, 108, 1–12, https://doi.org/10.1016/j.atmosenv.2015.02.058, 2015.

Moosmüller, H., Chakrabarty, R., and Arnott, W.: Aerosol light absorption and its measurement: A review, Journal of Quantitative Spectroscopy and Radiative Transfer, 110, 844–878, https://doi.org/10.1016/j.jqsrt.2009.02.035, 2009.

Nakajima, T., Campanelli, M., Che, H., Estellés, V., Irie, H., Kim, S.-W., Kim, J., Liu, D., Nishizawa, T., Pandithurai, G., Soni, V. K., Thana, B., Tugjsurn, N.-U., Aoki, K., Go, S., Hashimoto, M., Higurashi, A., Kazadzis, S., Khatri, P., Kouremeti, N., Kudo, R., Marenco, F., Momoi, M., Ningombam, S. S., Ryder, C. L., Uchiyama, A., and Yamazaki, A.: An overview of and issues with sky radiometer technology and SKYNET, Atmospheric Measurement Techniques, 13, 4195–4218, https://doi.org/10.5194/amt-13-4195-2020, 2020.

Offer, S., Hartner, E., Bucchianico, S. D., Bisig, C., Bauer, S., Pantzke, J., Zimmermann, E. J., Cao, X., Binder, S., Kuhn, E., Huber, A., Jeong, S., Käfer, U., Martens, P., Mesceriakovas, A., Bendl, J., Brejcha, R., Buchholz, A., Gat, D., Hohaus, T., Rastak, N., Jakobi, G., Kalberer, M., Kanashova, T., Hu, Y., Ogris, C., Marsico, A., Theis, F., Pardo, M., Gröger, T., Oeder, S., Orasche, J., Paul, A., Ziehm, T., Zhang, Z.-H., Adam, T., Sippula, O., Sklorz, M., Schnelle-Kreis, J., Czech, H., Kiendler-Scharr, A., Rudich, Y., and Zimmermann, R.: Effect of Atmospheric Aging on Soot Particle Toxicity in Lung Cell Models at the Air–Liquid Interface: Differential Toxicological Impacts of Biogenic and Anthropogenic Secondary Organic Aerosols (SOAs), Environmental Health Perspectives, 130, 027 003, https://doi.org/10.1289/EHP9413, 2022.

O'Neill, N. T., Eck, T. F., Smirnov, A., Holben, B. N., and Thulasiraman, S.: Spectral discrimination of coarse and fine mode optical depth, Journal of Geophysical Research: Atmospheres, 108, https://doi.org/10.1029/2002JD002975, 2003.

Ostro, B., Tobias, A., Karanasiou, A., Samoli, E., Querol, X., Rodopoulou, S., Basagaña, X., Eleftheriadis, K., Diapouli, E., Vratolis, S., Jacquemin, B., Katsouyanni, K., Sunyer, J., Forastiere, F., and Stafoggia, M.: The risks of acute exposure to black carbon in Southern Europe: results from the MED-PARTICLES project, Occupational and Environmental Medicine, 72, 123–129, https://doi.org/10.1136/oemed-2014-102184, 2015.

Paglione, M., Gilardoni, S., Rinaldi, M., Decesari, S., Zanca, N., Sandrini, S., Giulianelli, L., Bacco, D., Ferrari, S., Poluzzi, V., Scotto, F., Trentini, A., Poulain, L., Herrmann, H., Wiedensohler, A., Canonaco, F., Prévôt, A. S. H., Massoli, P., Carbone, C., Facchini, M. C., and Fuzzi, S.: The impact of biomass burning and aqueous-phase processing on air quality: a multi-year source apportionment study in the Po Valley, Italy, Atmospheric Chemistry and Physics, 20, 1233–1254, https://doi.org/10.5194/acp-20-1233-2020, 2020.

Petzold, A., Schloesser, H., Sheridan, P. J., Arnott, W. P., Ogren, J. A., and Virkkula, A.: Evaluation of Multiangle Absorption Photometry for Measuring Aerosol Light Absorption, Aerosol Science and Technology, 39, 40–51, https://doi.org/10.1080/027868290901945, 2005.

Petzold, A., Ogren, J. A., Fiebig, M., Laj, P., Li, S.-M., Baltensperger, U., Holzer-Popp, T., Kinne, S., Pappalardo, G., Sugimoto, N., Wehrli, C., Wiedensohler, A., and Zhang, X.-Y.: Recommendations for reporting black carbon measurements, Atmospheric Chemistry and Physics, 13, 8365–8379, https://doi.org/10.5194/acp-13-8365-2013, 2013.

Pikridas, M., Bezantakos, S., Močnik, G., Keleshis, C., Brechtel, F., Stavroulas, I., Demetriades, G., Antoniou, P., Vouterakos, P., Argyrides, M., Liakakou, E., Drinovec, L., Marinou, E., Amiridis, V., Vrekoussis, M., Mihalopoulos, N., and Sciare, J.: On-flight intercomparison of three miniature aerosol absorption sensors using unmanned aerial systems (UASs), Atmospheric Measurement Techniques, 12, 6425–6447, https://doi.org/10.5194/amt-12-6425-2019, 2019.

Pöschl, U.: Atmospheric Aerosols: Composition, Transformation, Climate and Health Effects, Angewandte Chemie International Edition, 44, 7520–7540, https://doi.org/10.1002/anie.200501122, 2005.

Putaud, J. P., Cavalli, F., Martins dos Santos, S., and Dell'Acqua, A.: Long-term trends in aerosol optical characteristics in the Po Valley, Italy, Atmospheric Chemistry and Physics, 14, 9129–9136, https://doi.org/10.5194/acp-14-9129-2014, 2014.

Putaud, J.-P., Pozzoli, L., Pisoni, E., Martins Dos Santos, S., Lagler, F., Lanzani, G., Dal Santo, U., and Colette, A.: Impacts of the COVID-19 lockdown on air pollution at regional and urban background sites in northern Italy, Atmospheric Chemistry and Physics, 21, 7597–7609, https://doi.org/10.5194/acp-21-7597-2021, 2021.

Regencia, Z. J. G., Dalmacion, G. V., Ligsay, A. D., and Baja, E. S.: Short-Term Cumulative Exposure to Ambient Traffic-Related Black Carbon and Blood Pressure: MMDA Traffic Enforcers' Health Study, International Journal of Environmental Research and Public Health, 18, 12 122, https://doi.org/10.3390/ijerph182212122, 2021.

Rosenfeld, D., Andreae, M. O., Asmi, A., Chin, M., de Leeuw, G., Donovan, D. P., Kahn, R., Kinne, S., Kivekäs, N., Kulmala, M., Lau, W., Schmidt, K. S., Suni, T., Wagner, T., Wild, M., and Quaas, J.: Global observations of aerosol-cloud-precipitation-climate interactions, Reviews of Geophysics, 52, 750–808, https://doi.org/10.1002/2013RG000441, 2014.

Russell, P. B., Bergstrom, R. W., Shinozuka, Y., Clarke, A. D., DeCarlo, P. F., Jimenez, J. L., Livingston, J. M., Redemann, J., Dubovik, O., and Strawa, A.: Absorption Angstrom Exponent in AERONET and related data as an indicator of aerosol composition, Atmospheric Chemistry and Physics, 10, 1155–1169, https://doi.org/10.5194/acp-10-1155-2010, 2010.

Saleh, R., Robinson, E. S., Tkacik, D. S., Ahern, A. T., Liu, S., Aiken, A. C., Sullivan, R. C., Presto, A. A., Dubey, M. K., Yokelson, R. J., Donahue, N. M., and Robinson, A. L.: Brownness of organics in aerosols from biomass burning linked to their black carbon content, Nature Geoscience, 7, 647–650, /10.1038/ngeo2220, 2014.

Sandradewi, J., Prévôt, A. S. H., Szidat, S., Perron, N., Alfarra, M. R., Lanz, V. A., Weingartner, E., and Baltensperger, U.: Using Aerosol Light Absorption Measurements for the Quantitative Determination of Wood Burning and Traffic Emission Contributions to Particulate Matter, Environmental Science & Technology, 42, 3316–3323, https://doi.org/10.1021/es702253m, 2008.

Shen, J., Bigi, A., Marinoni, A., Lampilahti, J., Kontkanen, J., Ciarelli, G., Putaud, J., Nieminen, T., Kulmala, M., Lehtipalo, K., and Bianchi, F.: Emerging Investigator Series: COVID-19 lockdown effects on aerosol particle size distributions in Northern Italy, Environmental Science: Atmospheres, 1, 214–227, https://doi.org/10.1039/D1EA00016K, 2021.

Shin, S.-K., Tesche, M., Müller, D., and Noh, Y.: Technical note: Absorption aerosol optical depth components from AERONET observations of mixed dust plumes, Atmospheric Measurement Techniques, 12, 607–618, https://doi.org/10.5194/amt-12-607-2019, 2019.

Sinyuk, A., Holben, B. N., Eck, T. F., Giles, D. M., Slutsker, I., Korkin, S., Schafer, J. S., Smirnov, A., Sorokin, M., and Lyapustin, A.: The AERONET Version 3 aerosol retrieval algorithm, associated uncertainties and comparisons to Version 2, Atmospheric Measurement Techniques, 13, 3375–3411, https://doi.org/10.5194/amt-13-3375-2020, 2020.

Slater, J. F. and Dibb, J. E.: Relationships between surface and column aerosol radiative properties and air mass transport at a rural New England site, Journal of Geophysical Research: Atmospheres, 109, https://doi.org/10.1029/2003JD003406, 2004.

Stavroulas, I., Pikridas, M., Grivas, G., Bezantakos, S., Liakakou, E., Kalkavouras, P., Veratti, G., Bigi, A., Gerasopoulos, E., Sciare, J., and Mihalopoulos, N.: Field evaluation of miniature absorption photometers in an Eastern Mediterranean urban environment, in: 11th International Aerosol Conference (IAC 2022), Athens, Greece, 2022.

Takemura, T. and Suzuki, K.: Weak global warming mitigation by reducing black carbon emissions, Scientific Reports, 9, 1–6, https://doi.org/10.1038/s41598-019-41181-6, 2019.

Thornhill, G. D., Collins, W. J., Kramer, R. J., Olivié, D., Skeie, R. B., O'Connor, F. M., Abraham, N. L., Checa-Garcia, R., Bauer, S. E., Deushi, M., Emmons, L. K., Forster, P. M., Horowitz, L. W., Johnson, B., Keeble, J., Lamarque, J.-F., Michou, M., Mills, M. J., Mulcahy, J. P., Myhre, G., Nabat, P., Naik, V., Oshima, N., Schulz, M., Smith, C. J., Takemura, T., Tilmes, S., Wu, T., Zeng, G., and Zhang, J.: Effective radiative forcing from emissions of reactive gases and aerosols – a multi-model comparison, Atmospheric Chemistry and Physics, 21, 853–874, https://doi.org/10.5194/acp-21-853-2021, 2021.

Thunis, P., Degraeuwe, B., Pisoni, E., Trombetti, M., Peduzzi, E., Belis, C. A., Wilson, J., and Vignati, E.: Urban PM 2.5 Atlas - Air Quality in European cities, Tech. Rep. EUR 28804 EN, Publications Office of the European Union, Luxembourg, https://doi.org/10.2760/336669, 2017.

Tuet, W. Y., Chen, Y., Xu, L., Fok, S., Gao, D., Weber, R. J., and Ng, N. L.: Chemical oxidative potential of secondary organic aerosol (SOA) generated from the photooxidation of biogenic and anthropogenic volatile organic compounds, Atmospheric Chemistry and Physics, 17, 839–853, https://doi.org/10.5194/acp-17-839-2017, 2017.

Twomey, S.: Pollution and the planetary albedo, Atmospheric Environment (1967), 8, 1251–1256, https://doi.org/10.1016/0004-6981(74)90004-3, 1974.

Uria-Tellaetxe, I. and Carslaw, D. C.: Conditional bivariate probability function for source identification, Environmental Modelling & Software, 59, 1–9, https://doi.org/10.1016/j.envsoft.2014.05.002, 2014.

Vecchi, R., Bernardoni, V., Valentini, S., Piazzalunga, A., Fermo, P., and Valli, G.: Assessment of light extinction at a European polluted urban area during wintertime: Impact of PM1 composition and sources, Environmental Pollution, 233, 679–689, https://doi.org/10.1016/j.envpol.2017.10.059, 2018.

Veratti, G., Fabbi, S., Bigi, A., Lupascu, A., Tinarelli, G., Teggi, S., Brusasca, G., Butler, T., and Ghermandi, G.: Towards the coupling of a chemical transport model with a micro-scale Lagrangian modelling system for evaluation of urban NO_x levels in a European hotspot, Atmospheric Environment, 223, 117 285, https://doi.org/https://doi.org/10.1016/j.atmosenv.2020.117285, 2020.

Veratti, G., Bigi, A., Lupascu, A., Butler, T., and Ghermandi, G.: Urban population exposure forecast system to predict NO_2 impact by a building-resolving multi-scale model approach, Atmospheric Environment, 261, 118 566, https://doi.org/https://doi.org/10.1016/j.atmosenv.2021.118566, 2021.

Veratti, G., Stortini, M., Amorati, R., Bressan, L., Giovannini, G., Bande, S., Bissardella, F., Ghigo, S., Angelino, E., Colombo, L., Fossati, G., Malvestiti, G., Marongiu, A., Dalla Fontana, A., Intini, B., and Pillon, S.: Impact of NO_x and NH_3 Emission Reduction on Particulate Matter across Po Valley: A LIFE-IP-PREPAIR Study, Atmosphere, 14, 762, https://doi.org/10.3390/atmos14050762, 2023.

Viana, M., Rivas, I., Reche, C., Fonseca, A. S., Pérez, N., Querol, X., Alastuey, A., Álvarez Pedrerol, M., and Sunyer, J.: Field comparison of portable and stationary instruments for outdoor urban air exposure assessments, Atmospheric Environment, 123, 220–228, https://doi.org/10.1016/j.atmosenv.2015.10.076, 2015.

Virkkula, A., Mäkelä, T., Hillamo, R., Yli-Tuomi, T., Hirsikko, A., Hämeri, K., and Koponen, I. K.: A Simple Procedure for Correcting Loading Effects of Aethalometer Data, Journal of the Air & Waste Management Association, 57, 1214–1222, https://doi.org/10.3155/1047-3289.57.10.1214, 2007.

Visser, B., Röhrbein, J., Steigmeier, P., Drinovec, L., Močnik, G., and Weingartner, E.: A single-beam photothermal interferometer for in situ measurements of aerosol light absorption, Atmospheric Measurement Techniques, 13, 7097–7111, https://doi.org/10.5194/amt-13-7097-2020, 2020.

Vogelezang, D. H. P. and Holtslag, A. A. M.: Evaluation and model impacts of alternative boundary-layer height formulations, Boundary-Layer Meteorology, 81, 245–269, https://doi.org/10.1007/BF02430331, 1996.

Wang, R.: Global emission inventory and atmospheric transport of Black Carbon, Springer Theses, Springer Berlin Heidelberg, Berlin, Heidelberg, https://doi.org/10.1007/978-3-662-46479-3, 2015.

Wang, R., Balkanski, Y., Boucher, O., Ciais, P., Schuster, G. L., Chevallier, F., Samset, B. H., Liu, J., Piao, S., Valari, M., and Tao, S.: Estimation of global black carbon direct radiative forcing and its uncertainty constrained by observations, Journal of Geophysical Research: Atmospheres, 121, 5948–5971, https://doi.org/10.1002/2015JD024326, 2016a.

Wang, X., Heald, C. L., Sedlacek, A. J., de Sá, S. S., Martin, S. T., Alexander, M. L., Watson, T. B., Aiken, A. C., Springston, S. R., and Artaxo, P.: Deriving brown carbon from multiwavelength absorption measurements: method and application to AERONET and Aethalometer observations, Atmospheric Chemistry and Physics, 16, 12 733–12 752, https://doi.org/10.5194/acp-16-12733-2016, 2016b.

Weingartner, E., Saathoff, H., Schnaiter, M., Streit, N., Bitnar, B., and Baltensperger, U.: Absorption of light by soot particles: determination of the absorption coefficient by means of aethalometers, Journal of Aerosol Science, 34, 1445–1463, https://doi.org/10.1016/S0021-8502(03)00359-8, intercomparison of Soot Measurement Techniques, 2003.

Weitekamp, C. A., Stevens, T., Stewart, M. J., Bhave, P., and Gilmour, M. I.: Health effects from freshly emitted versus oxidatively or photochemically aged air pollutants, Science of The Total Environment, 704, 135 772, https://doi.org/https://doi.org/10.1016/j.scitotenv.2019.135772, 2020.

West, J. J., Cohen, A., Dentener, F., Brunekreef, B., Zhu, T., Armstrong, B., Bell, M. L., Brauer, M., Carmichael, G., Costa, D. L., Dockery, D. W., Kleeman, M., Krzyzanowski, M., Künzli, N., Liousse, C., Lung, S.-C. C., Martin, R. V., Pöschl, U., Pope, C. A., Roberts, J. M., Russell, A. G., and Wiedinmyer, C.: What we breathe impacts our health: improving understanding of the link between air pollution and health, Environmental Science & Technology, 50, 4895–4904, https://doi.org/10.1021/acs.est.5b03827, 2016.

WHO: WHO global air quality guidelines. Particulate matter (PM2.5 and PM10), ozone, nitrogen dioxide, sulfur dioxide and carbon monoxide., Tech. rep., World Health Organization, Geneva, CH, 2021.

Yang, J., Sakhvidi, M. J. Z., de Hoogh, K., Vienneau, D., Siemiatyck, J., Zins, M., Goldberg, M., Chen, J., Lequy, E., and Jacquemin, B.: Long-term exposure to black carbon and mortality: A 28-year follow-up of the GAZEL cohort, Environment International, 157, 106 805, https://doi.org/10.1016/j.envint.2021.106805, 2021.

Yus-Díez, J., Bernardoni, V., Močnik, G., Alastuey, A., Ciniglia, D., Ivančič, M., Querol, X., Perez, N., Reche, C., Rigler, M., Vecchi, R., Valentini, S., and Pandolfi, M.: Determination of the multiple-scattering correction factor and its cross-sensitivity to scattering and wavelength dependence for different AE33 Aethalometer filter tapes: a multi-instrumental approach, Atmospheric Measurement Techniques, 14, 6335–6355, https://doi.org/10.5194/amt-14-6335-2021, 2021.

Zanatta, M., Gysel, M., Bukowiecki, N., Müller, T., Weingartner, E., Areskoug, H., Fiebig, M., Yttri, K. E., Mihalopoulos, N., Kouvarakis, G., Beddows, D., Harrison, R. M., Cavalli, F., Putaud, J. P., Spindler, G., Wiedensohler, A., Alastuey, A., Pandolfi, M., Sellegri, K., Swietlicki, E., Jaffrezo, J. L., Baltensperger, U., and Laj, P.: A European aerosol phenomenology-5: Climatology of black carbon optical properties at 9 regional background sites across Europe, Atmospheric Environment, 145, 346–364, https://doi.org/10.1016/j.atmosenv.2016.09.035, 2016.

Zhang, A., Wang, Y., Zhang, Y., Weber, R. J., Song, Y., Ke, Z., and Zou, Y.: Modeling the global radiative effect of brown carbon: a potentially larger heating source in the tropical free troposphere than black carbon, Atmospheric Chemistry and Physics, 20, 1901–1920, https://doi.org/10.5194/acp-20-1901-2020, 2020.

Zhang, X., Li, L., Chen, C., Zheng, Y., Dubovik, O., Derimian, Y., Lopatin, A., Gui, K., Wang, Y., Zhao, H., Liang, Y., Holben, B., Che, H., and Zhang, X.: Extensive characterization of aerosol optical properties and chemical component concentrations: Application of the GRASP/Component approach to long-term AERONET measurements, Science of The Total Environment, 812, 152 553, https://doi.org/10.1016/j.scitotenv.2021.152553, 2022.

Zhu, C., Miyakawa, T., Irie, H., Choi, Y., Taketani, F., and Kanaya, Y.: Light-absorption properties of brown carbon aerosols in the Asian outflow: Implications of a combination of filter and ground remote-sensing observations at Fukue Island, Japan, Science of The Total Environment, 797, 149 155, https://doi.org/10.1016/j.scitotenv.2021.149155, 2021.